# A study of Optically Pumped Nuclear Magnetic Polarization on Gallium Arsenide

by

YUNPU LI

A dissertation submitted to the Graduate Faculty in Physics in partial fulfillment of the requirements for the degree of Doctor of Philosophy,

The City University of New York

2012

This manuscript has been read and accepted for the Graduate Faculty in Physics in Satisfaction of the dissertation requirement for the degree of Doctor of Philosophy.

| | |
|---|---|
| | Prof. Carlos A. Meriles |
| _____ | _____ |
| Date | Chair of Examining Committee |
| | Prof. Igor L. Kuskovsky |
| _____ | _____ |
| Date | Executive Officer |

Prof. Igor L. Kuskovsky

Prof. Maria Tamargo

Dr. Shiping Guo

Supervisory Committee

THE CITY UNIVERSITY OF NEW YORK

Abstract

A study of Optically Pumped Nuclear Magnetic Polarization on Gallium Arsenide

By

Yunpu Li

Advisor: Prof. Carlos A. Meriles

This thesis aims to study the dynamic process of optically pumped nuclear spin polarization on Gallium Arsenide. First of all, the time-resolved optical Faraday rotation is applied to observe the electron spin dynamics in the presence of the nuclear magnetic field. And then the optically-pumped NMR is measured on different parameters, including the dependences of light helicity, irradiation intensity, photon energy, illumination time and temperature. We report a new phenomenology at low irradiation intensity. A nuclear polarization model combining hyperfine and quadrupolar relaxation is developed, with experimental data supported. By exploiting the two competing mechanism on various photon energies, illumination intensity and NMR pulse sequences, we use high field stray-field NMR imaging to realize all-optical creation of three-dimensional patterning of positive and negative nuclear polarization on the micron length scale. Finally, the effect of nuclear spin diffusion effect is investigated. We demonstrate in a remarkable way the unambiguous evidence of diffusion, which results in a great enhancement of quadrupolar relaxation in the nanometer scale.

**Acknowledgments**

First and foremost I offer my sincerest gratitude to my supervisor, Prof. Carlos Meriles, who has supported me throughout my entire Ph.D. study with his knowledge and patience. His expertise, understanding, and encouragement add considerably to my Ph.D. experience. It is him that guides me in the field of NMR and supports me in building up the knowledge and confidence. I am a blunt student, and he put a lot of effects on me. Without him this thesis would not have been completed or written. I also appreciate his support to me in winning the Outstanding Teaching Assistant of the Year in competition.

I must also acknowledge Prof. Jeff Reimer and his student Jonathon King at UC Berkeley, who contributed in the theoretical part of this thesis. Appreciation also goes to Prof. Maria Tamargo, her student Qiang Zhang and Le Peng, who collaborated with me in Optical Pumping project and other projects that are not displayed in this thesis.

A very special thanks goes out to my boyfriend Jian Li, without whose love and encouragement I would not have completed this thesis. Jian Li is the one who truly made a difference in my life. It was him that spent almost every sleepless night with me running Optical Pumping experiments, even though he does not work in my lab. I owe him my eternal gratitude.

I would also like to thank my lab members for exchanges of knowledge, skills, and venting of frustration during my Ph.D. program, which helped enrich the experience: Denial Pagalalo, Wei Dong, Bo Li and Abdelghani Laraoui, S. Fisher and Xuejun Liu.

Thanks also go out to my friends who provided me with advice at times of critical need: Rui zhang, Wei Liu, Yuliang Jin, Lukas Zhao and Bo Wen.

I would like to thank the other members of my committee for the assistance they provided at all levels of the research project.

The Department of Physics has provided the support and equipment I have needed to produce and complete my thesis and the NSF has funded my studies.

Finally, I would like to thank my family for the support they provided me through my entire life.

**Contents**

**List of Figures**

## I. Introduction

The concept of spin was first proposed by Wolfgang Pauli[1]. Early in 1922, the Stern-Gerlach experiment[2] (in the context of the deflection of a particle atoms beam through an inhomogeneous magnetic field) indicates that the particles possess an intrinsic angular momentum. In 1925, George Uhlenbeck and Samuel Goudsmit suggested an interpretation of electrons spinning around their own axis[3], which Ralph Kronig also saw but did not publish. The mathematical theory was worked out by Pauli in 1927. When Paul Dirac worked out the relativistic quantum mechanics in 1928, electron spin became an essential part thereof.

Spin is a type of angular momentum. In classical point of view, as a qualitative concept, one can exert a kind of "torque" on a particle with spin by placing it in a magnetic field which acts on the electron's intrinsic magnetic dipole moment. The result is that the spin vector undergoes precession, like a classical gyroscope. In quantum mechanics, spin is an intrinsic physical property. It is convenient to describe by quantum number $s$, as $s = n/2$, where $n$ is any non-negative integer.

Particles with spin can possess a magnetic dipole moment, which can be experimentally observed in several ways. The intrinsic magnetic moment $\mu$ of an elementary particle with charge $q$, mass $m$, and spin angular momentum $S$, is $\mu = g\frac{q}{2m}S = \gamma \mathrm{h} S$, where the dimensionless quantity $g$ is called the g-factor and $\gamma$ is the gyromagnetic ratio.

Typical questions for the control of spin include (a) what is an effective approach to generate a steady-state, non-Boltzmann spin population in a system? (b) How long is the system able to remember its spin orientation? And (c) how can spin be detected?[4]

Nuclear magnetic resonance (NMR) was first described and measured in molecular beams by Isidor Rabi in 1938[5]. In 1946, Felix Bloch and Edward Mills Purcell expanded the technique for use on liquids and solids.

All nucleons have the intrinsic quantum property of spin. The overall spin of the nucleus is determined by the spin quantum number $I$. A non-zero spin is always associated with a non-zero magnetic moment $\mu$ via the relation $\mu = \gamma \mathrm{h} I$. Those nuclides (with some rare exceptions) that have either odd numbers of protons or odd numbers of neutrons, also have non-zero nuclear magnetic moments, and also have non-zero magnetic dipole and some may have non-zero quadrupole moments; therefore, such nuclides exhibit any NMR absorption spectra.

If a nucleus of spin 1/2 is placed in a magnetic field, for example, $^1$H, the energy of a magnetic moment $\mu$ in a magnetic field $B_0$ is given by $H = -\mu B_0$. Usually, $B_0$ is set to be along the z axis. As a result, different nuclear spin states have different energies in a non-zero magnetic field. For a spin 1/2 particle, the two spin states are aligned either with or against the magnetic field. The eigenvalue of each state is $E_m = m\mathrm{h}\gamma B_0$. The energy difference between the two states is, $\Delta E = \gamma \mathrm{h} B_0$, and this difference results in a small population bias toward the lower energy state. The net magnetization, M, of a system containing N nuclear spins will be proportional to the expectation value of the spin angular momentum in z-direction $< I_z >$, $M = N\gamma \mathrm{h} < I_z >$. According to Boltzmann statistical mechanics, at thermal equilibrium, $< I_z >= \frac{\sum_m m e^{-\gamma \mathrm{h} m B_0 / kT}}{\sum_m e^{-\gamma \mathrm{h} m B_0 / kT}}$, where k is the Boltzmann constant and T is temperature .

In simple terms, an oscillating field $B_1$, which is perpendicular to $B_0$, will deflect the M from its thermal equilibrium position, as long as $B_1$ is oscillating near the frequency $\omega = \gamma B_0$. The electromagnetic radiation, such as a short square pulse, contains a range of frequencies centered at the same frequency as spin resonance, with the bandwidth of excitation being inversely proportional to the pulse duration. The energy generator is usually a coil, which itself is a detection device. Applying such a pulse to nuclear spins simultaneously excites all the single-quantum NMR transitions. In terms of the net magnetization vector M, this corresponds to tilting the magnetization vector away from its equilibrium position (aligned along the external magnetic field). The out-of-equilibrium magnetization vector precesses about z-axis at the NMR frequency. When one by one spins return to the ground state, they emit the electromagnetic radiation, which induces a current in the pickup coil, creating an electrical signal oscillating at the NMR frequency. This signal is known as the free induction decay (FID) containing the vector-sum of the NMR responses from all the excited spins, and the Fourier transformed FID is the NMR spectrum. More specifically, a $\pi/2$ pulse is to deflect the spins into x-y plane, and it is usually adopted as the excitation pulse prior to the acquisition.

The conventional NMR is a powerful probe of chemical structures, electron properties and so on. It has been widely used in physics, chemistry, biology, medication and those cross-disciplines. However, the lack of sensitivity of detection is a principle limitation. For spin 1/2 $^1$H, $\gamma = 26.7519\times10^7 rad/Ts$, in presence of $B_0 = 9.4T$ at room temperature T=300K, $< I_z >= \dfrac{-\frac{1}{2}e^{\gamma \mathrm{h} B_0/2kT} + \frac{1}{2}e^{-\gamma \mathrm{h} B_0/2kT}}{e^{\gamma \mathrm{h} B_0/2kT} + e^{-\gamma \mathrm{h} B_0/2kT}} = \frac{1}{2}\tanh(-\dfrac{\gamma \mathrm{h} B_0}{2kT}) \approx 5\times10^{-5}$ S.I. unit. That means only one out of $10^4$ nuclei is spin polarized.

Thus, due to the fact that the electromagnetic energy involved in the detection is that of the transition induced, it requires active nuclear moments in large numbers ($10^7$ or more) to have acceptable signal-to-noise ratios. This in turn makes it necessary to use bulk samples.[6]

The signal-to-noise ratio is always considered as the fundamental restriction for an experiment in estimating the amount of material, S/N: $S/N \propto N\gamma_e\sqrt{\gamma_d{}^3 B_0 t}$, where N is the number of nuclear spins being observed, $\gamma_e$ is the gyromagnetic ratio of the spin being excited, $\gamma_d$ is the gyromagnetic ratio of the spin being detected, and t is the experiment acquisition time.[7] Other factors involved in S/N are the probe filling factor (e.g., how much of the coil detection volume is filled with sample), and various other probe and receiver factors.

The development in technologies, such as affordable super-conducting high-field magnets, magic angle spinning, innovated detection device and complicated pulse sequences expand the scope of NMR studies. On the other hand, some methodologies, such as optical pumping that can enhance the nuclear polarization by a factor of $10^5$ or more, have been applied on several systems, showing great potentials in related spintronics detections and quantum computing device manufacturing.

The optical pumping of nuclear spins is a dynamic polarization of nuclear spins, which results from the polarization transferring between electron spin and nuclear spin through electron-nuclear hyperfine interaction, under circularly polarized light illumination. The pioneer experiment of optically pumped enhancement on nuclear spins polarization in solid state systems was accomplished by Georgs Lampel.[8] In the experiments, a xenon lamp of 1 W with photon energy at about 1.2 eV was used to illuminate an n-doped Si sample at 77K.

After 37 hours of illumination with unpolarized light in a 0.16 T field, the amplitude of $^{29}Si$ NMR signal was observed to be enhanced by a factor of 5.6 and inverted in sign relative to the thermal equilibrium signal in the same field. After 21 h of irradiation with circular polarized light in a field of only 0.1 mT, the NMR signal was equivalent to the thermal equilibrium value in a field of 1.5 T.

In 1990s, Barrett et al. initialed Optically Pumped NMR (OPNMR) experiments on multiple quantum wells GaAs/$Al_xGa1_{-x}As$, examining the dependence on various parameters (photon energy, light power and helicity, and temperature).[9,10,11] Plus, the dependence of OPNMR signal on parameters was invested in different materials, e.g., GaAs[12,13,14,15,16,17,18], InP[19,20,21], CdS[22], and CdTe[23,24]. Recently, OPNMR researches have been focused on exploring the mechanisms of some optical pumping phenomena, including some electron states at fractional quantum Hall and integer quantum Hall regimes[7,25], hyperfine shifts[7,8], dipolar order[26] and so on.

Moreover, other optical pumping experiments on semiconductors made use of optical method to indirectly detect nuclear polarization, namely, optically detected NMR (ODNMR). ODNMR has extreme spatial selectivity, unlike the conventional NMR which can only see the bulk average magnetization. Therefore, ODNMR is of great value to characterize defects and impurities in specific structures. When nuclear spins are strongly polarized by electron spins via optical pumping, they exert a magnetic field (nuclear hyperfine field) on electron spins. By altering the nuclear spins polarization with the external electromagnetic energy—e.g., RF pulses—the magnitude and direction of the nuclear hyperfine field are modified, resulting in the change of electron spin precession, dephasing, and

photoluminescence.

Gallium Arsenide (GaAs), which is the most common representative of a large class of III-V and II-VI zinc-blende semiconductors, is widely used in the manufacture of spintronic devices. With its zinc-blende crystal structure, GaAs has superb property in photon absorption and emission so that its various forms (bulk, quantum wells) are well studied on the topic of optical pumping.

The optical detected and RF pulse detected (via RF coil) optical pumping on bulk GaAs will be discussed hereby.

## II. Theory

### 2.1. Generating electron spin polarization optically

The importance of generating non-Boltzmann spin population is not limited to spintronic device application; it can also be used as a sensitive spectroscopic tool to study nuclear spins. Non-equilibrium spin is the result of some kind of pumping source as transport, optical, or resonance methods. Once the pumping is turned off, the spin will relax to its equilibrium value.[4] The optical pumping is an optical method to generate non-equilibrium spin polarization and accumulate spins. Optical pumping in semiconductor is a well-established technique,[27] that is, the angular momentum of absorbed circularly polarized light is transferred to the medium. A simple reversal of the illumination helicity (from left- to right-circularly polarized) also reserves the sign of the electron spin polarization.

The basic principles of optical pumping can be illustrated by the example of GaAs, which has direct gap at Brillouin zone center. The electronic band structure is showed in Fig. 2.1(a). The conduction band wave functions have orbital angular momentum L=0, spin angular momentum S=1/2, and a total angular momentum J=1/2. The valence band wave functions have orbital angular momentum L=1, spin angular momentum S=1/2, and a total angular momentum J=1/2 or 3/2. The band gap of GaAs at the center of the Brillouin zone $\Gamma$ is $E_g = 1.42eV$ at room temperature. Because of the spin-orbit coupling, the valance band is split into the heavy/light hole valance band (J=3/2) and a split-off subband (J=1/2), with the energy $\Delta_{so} = 0.34eV$ . For the illumination with circularly polarized light, electrons

are excited to conduction band (J=1/2) via the selection rule in Fig. 2.1(b), $\Delta m_j = \pm 1$. For example, for the illumination of right circularly polarized light $\sigma^+$, at the energy of $E = \mathrm{h}\omega$, $E_g \le E \le E_g + \Delta_{so}$, electrons will be excited from the valence bands to the conduction band, i.e., from valence band heavy hole ($m_j$=-3/2) to conduction band ($m_j$=-1/2), and from valance band light hole ($m_j$=-1/2) to conduction band ($m_j$=1/2), with the rate of 3:1, which is noted in Fig. 2.1 b by the solid lines. The numbers in the circle are the transition rates. Denoting by $n^+$ and $n^-$ the density of electron polarized parallel ($m_j$=1/2) and anti-parallel ($m_j$=-1/2) to the direction of light propagation, the spin polarization of the sample is defined as $P_n = (n_+ - n_-)/(n_+ + n_-)$.

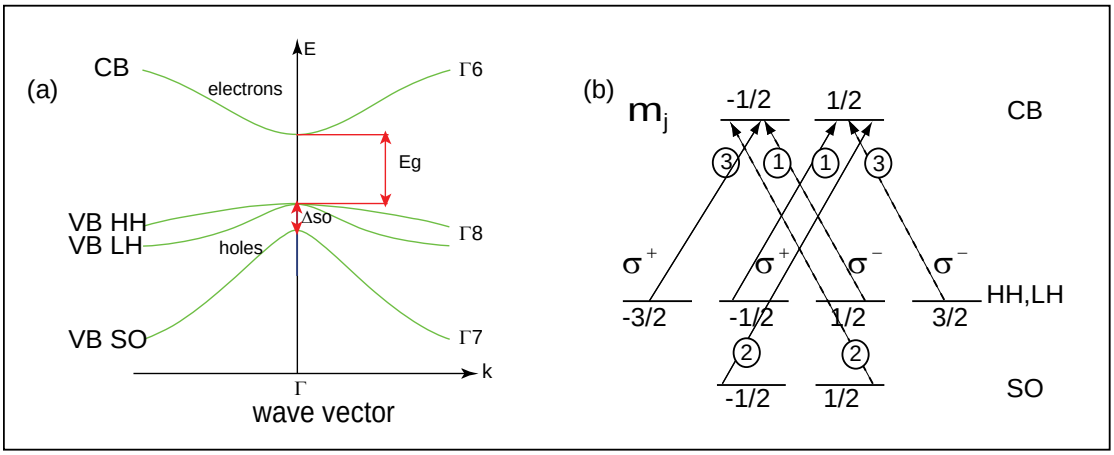


Fig. 2.1 Electrical energy level diagram and selection rule for GaAs under illumination of circularly polarized light. The numbers in circles in (b) denote the rated for each transition.

For the example of right circularly polarized illumination, the spin polarization of the sample is $P_n = (1-3)/(1+3) = -1/2$. The spin is oriented against the direction of light propagation, since there are more transitions from the heavy hole that from the light hole bands.

If the excitation involves the transitions from the spilt-off band, that is, $E > E_g + \Delta_{so}$, the

electrons will not be spin polarized.

## 2.2. Optical Pumping of nuclear spins

Optical pumping (OP) of nuclear spins was first theoretically proposed by Kastler[28] whereby large population bias in the ground states of atoms can change absorption of polarized light. Georgs Lampel's work[5] on $^{29}Si$ in 1968 showed that nuclear spin polarization could be drove out of thermal equilibrium by simply light irradiation.

Let us take GaAs as the example, electron spin polarization is generated by the circularly polarized excitation, which is not the thermal equilibrium value at that temperature. Thus, via electron-nuclear hyperfine interaction, electron spins are transferred to nuclear spin reservoir. At low temperature, electron spin relaxation time is much shorter than that of nuclear spin, so that the nuclear spin polarization can be accumulated via many excitation cycles. In this case, the nuclear spin polarization can be pumped either positively or negatively, depending on the helicity of the pumping light. The nuclear spin magnetization can be measured and manipulated by various methods, e.g., via pulsed NMR.

## 2.3. Optical Faraday rotation

Optical Faraday rotation (OFR) in a macroscopic picture is the rotation of axis of the linear polarized light when it propagates through a magnetized medium (Fig. 2.2 (a)). The rotation angle

$$\theta = VBl, \tag{2-1}$$

Where $\boldsymbol{B}$ is the magnetic field and $l$ is the length of the sample along the path of light propagation, and $V$ is the Verdet constant.

A modern picture involves the quantum-mechanical response of an atom to a magnetic field. In this picture (Fig. 2.2 (b)), the atomic absorption and dispersion are both affected by the magnetic field, and in this sense the Faraday rotation is to dispersion what the Zeeman effect is to absorption (or emission). A linear polarized beam can be decomposed to two oppositely circularly polarized beams, which are assumed to propagate independently. Each of the two circularly polarized fields has its own index of refraction and attenuation coefficient. In the presence of a magnetic field, the atom in the medium shows the "normal" Zeeman effect. So each polarization will propagate with its own index of refraction and attenuation constant as a function of wavelength (transition frequency). The equation (2-1) can be rewritten as $\theta = \frac{1}{\lambda}\frac{e}{2m_e}\frac{dn}{d\nu}Bl$ to the lowest order in $B$, where $\lambda$ is the wavelength, $n$ is the index of refraction, and $\nu$ is the transition frequency. At the Bohr frequency of the transition, the Faraday rotation angel reaches its maximum (Fig. 2.2 (c)).[29]

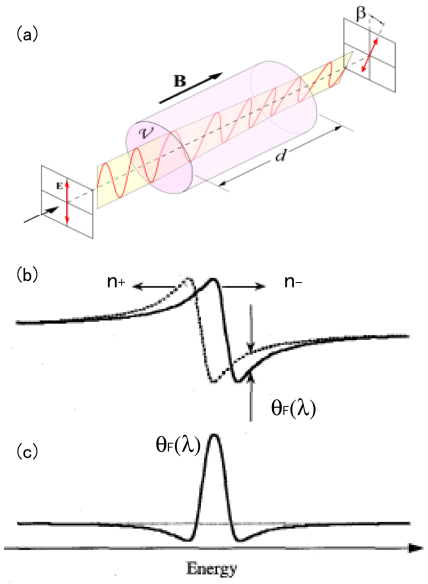


Fig. 2.2 Faraday rotation angel.

The aforementioned Optical Pumping of nuclear spin can also be detected via optical Faraday rotation by observing the electron spin precession since the polarized nuclei can exert large magnetic fields on electron spins.

This basic theory is not limited to the case of Faraday rotation, which is for the transmission of light through the sample. The same experiment can be performed in reflection mode (Kerr geometry). Kerr rotation measurements may suit to large scale sample characterization and analysis or on situation where a substrate prohibitively absorbs the light in the range of interest.

## III. Optically Pumped NMR Experiments on Gallium Arsenide

The advanced feature of GaAs is that it has a direct band gap, which means its electron spin can be highly polarized under circularly excitation. Thus, the degree of nuclear spin polarization can be enhanced by orders of magnitude via hyperfine interaction with non-equilibrium electron spin system. [11,30,31] The optical pumping has to take place at liquid helium temperature for practical purpose. The temperature dependence of band gap energy for GaAs has been well studied[32], which is 1.507 eV at 78K, and 1.519 eV at 5K.

### 3.1. Optical Pumping detected via time-resolved Optical Faraday Rotation

The time-resolved Optical Faraday Rotation (OFR) was adopted to detect the motion of electron spins in presence of a total magnetic field. The experimental setup of time-resolved OFR is shown in Fig. 3.1. In the experiment, a modelock Ti:sapphire laser with a duration of 200 fs and a repetition rate at 76 MHz was used. The laser was split into a pump beam and a probe beam by a beam splitter. The pump was modulated at 100 kHz by PEM with two crossed polarizers, while the probe was chopped at 5 kHz and one tenth of the pump intensity. The lock-in amplifier reading the signal from the balanced detectors at the reference frequency of 95 kHz, was therefore sensitive only to the pump-induced changes in the measured Faraday rotation of the probe beam. A lens was used to focus and overlap the pump and probe beams on the sample. At the zero-delay of the translation stage, the electron spin polarization of sample was induced and then relaxed. The probe beam was split by a

Glan-laser polarizer. The combination of the half-wave plate and Glan-laser polarizer was to orient the polarization plane of the probe beam so that, in the absence of Faraday rotation, the two detectors were balanced. The laser repetition interval $t_{rep}$ was ~13ns, i.e., the probe pulse only met the pump pulse at the zero-delay position on the sample, in a period of 13ns. The sample was placed in a continuous flow cryostat (OXFORD) and in good thermal contact with the cold finger for low temperature purpose.

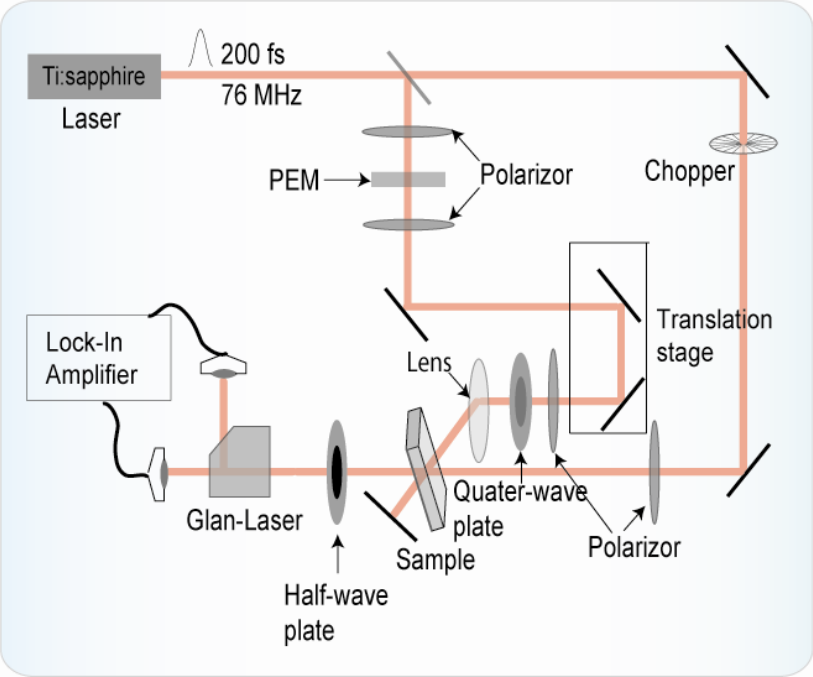


Fig. 3.1. Experimental set-up of time-resolved Faraday rotation.

The time-resolved OFR signal at room temperature is given in Fig. 3.2, at the photon energy of 1.393 eV (890nm), which is a little bit lower than the band gap energy (1.42eV)[32] at room temperature. The signals are symmetric for right- and left-circularly polarized illumination. The signal can be fit by the empirical formula $\exp(-t/\tau_{1s})$, where $\tau_{1s}$ is the electron spin relaxation time, about 70 ps at room temperature.

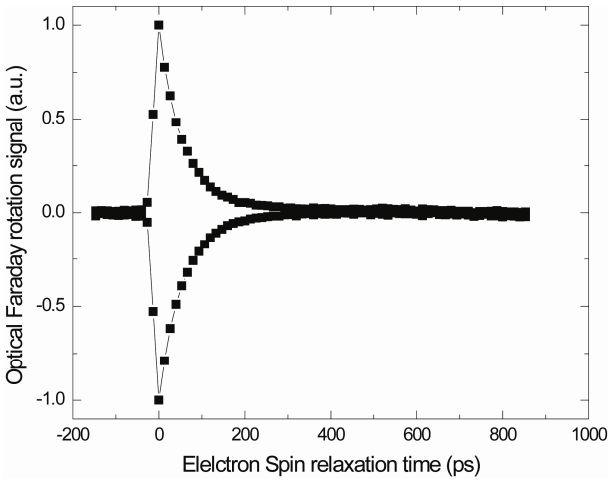


Fig. 3.2. OFR signal as a function of time for GaAs at room temperature, showing the electron spin relaxation time.

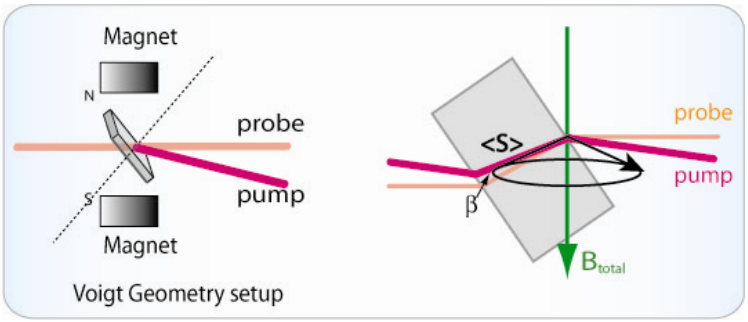


Fig. 3.3. Voigt geometry. Electron spins precess with the total magnetic filed.

Assuming there is an external magnetic field exerting on the sample (Voigt geometry, Fig. 3.3), the electron spin presseses along this field. The precession frequency is $\omega = \mu B_{total} g / \mathrm{h} = \gamma g B_{total}$ . As shown in appendix, what is measured by the detectors is the projection of the precession along the detection, equates to $\exp(-t/\tau_{1s})\cos\beta$ , where

$$\cos\beta = \cos\theta\cos\varphi + \sin\theta\cos(\omega t)\,, \qquad (3\text{-}1)$$

where $\beta$ is the angle between the pump and probe, $\theta$ is the angle between $B$ and the pump,

and $\varphi$ is the angle between $B$ and probe, that is, $\varphi = \beta + \theta$. The time-resolved OFR signal is strongly imposed by the angles. A simulation of angle dependence is shown in Fig. 3.4, for bulk GaAs at 78K in an external field of 6500G, and the electron g-factor is -0.41.

With the setup in Fig. 3.3, for the Si-doped (n-type) GaAs bulk (carrier concentration $2.6\times10^{16}/cm^3$), at 78K, the OFR signal is presented in Fig. 3.5. Considering the index of refractive for the sample $n = 3.3$, in the case of incident angle of probe at proximately $45^o$ ($\varphi = 57.35^o$), and pump at $55^o$ ($\theta = 59.37^o$). The fit gives parameters as $B = 6456G$ perpendicular with respect to the probe, and $\theta = 61.87^o$, and $\varphi = 55.59^o$. We claim that the experimental curve is perfectly reproduced.

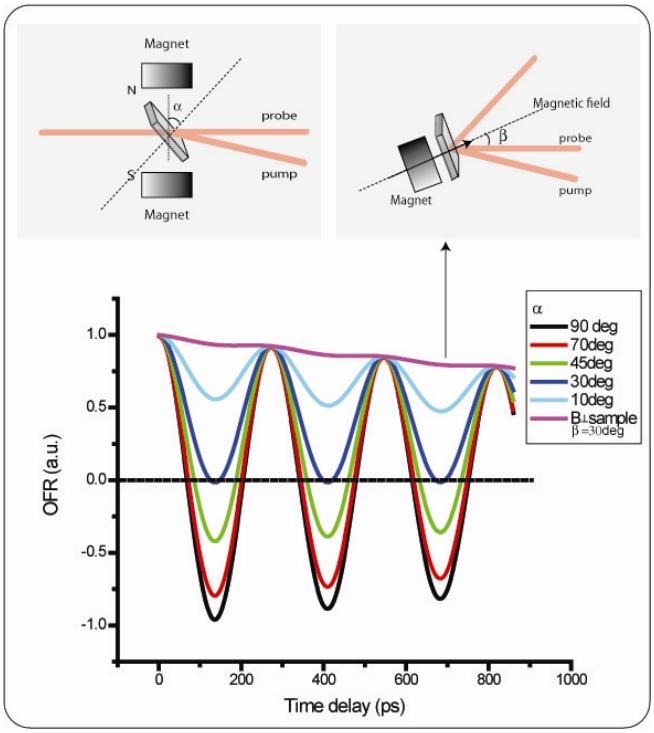


Fig. 3.4 OFR in Voigt geometry as a function of incident angle.

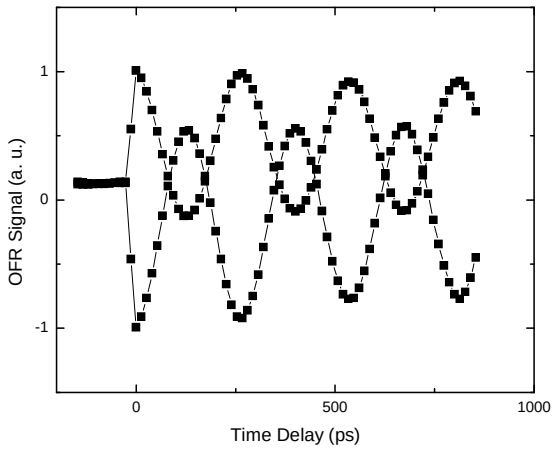


Fig. 3.5. GaAs in Voigt geometry at 78K.

At 4.4K, the nuclear spin magnetization is generated by optical pumping. This magnetic field, whose direction and magnitude are dependent on the helicity of the illumination light, affects the electron spin precession in additional to the external field. The time-resoled OFR signal after 300 s of pumping at 1.50 eV (825nm) is shown in Fig. 3.6. The electron g-factor is -0.44. Fit by equation (3.1), the shifted frequency is about $\Delta\omega = 0.0038\times10^{12} rad$ , which gives the magnitude of the difference of the nuclear field ( $B_{N+} - B_{N-}$ ) almost 980G.

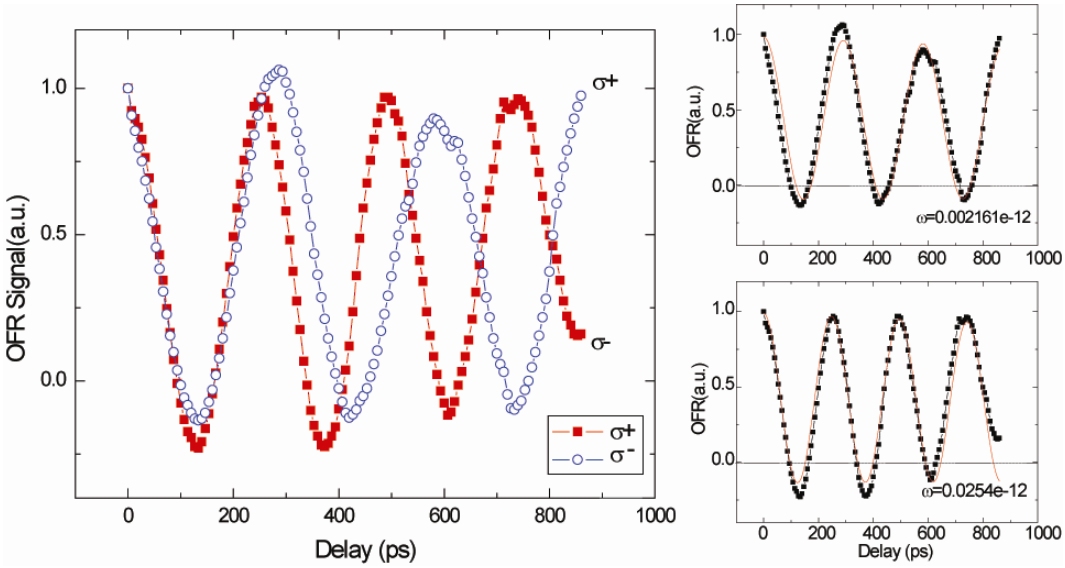


Fig. 3.6. Optical pumping OFR of doped GaAs at 4.4k.

The manipulation of nuclear spins via electrical and optical means can be achieved[33,34,35,36]. Awschalom et al have demonstrated all-optical methods to tip nuclear moments in n-type GaAs crystal. They used periodical excited electron spins to depolarize the nuclear spin field instead of RF fields.[30] Ohno et al have demonstrated the complete light induced resonance spectra as well as the quadrupolar splittings in GaAs quantum wells.[31] They also have demonstrated local manipulation and detection by optical method combined with pulsed-NMR.[32] Multiple NMR pulses can be applied to control the population and the phase of quadrupolar splitting in $^{75}$As. This method not only can be applied to study the phase coherence in quantum states, but also the readout of quantum information stored in multilevel nuclear spins in dense memory devices.[33]

3.2. Optically Pumped NMR on Semi-insulating GaAs

All the constituent atoms in GaAs, $^{71}$Ga, $^{69}$Ga, and $^{75}$As have nuclear spin 3/2. We used Optically Pumped NMR (OPNMR) to monitor the dynamic polarization of nuclear spins in bulk GaAs at 9.4 T.

(1) A model combined with Hyperfine and Quadrupolar relaxation

The sample was a bulk semi-insulating GaAs (350 $\mu m$ in thickness, surfaces orientation [100], resistivity greater than $10^7\,\Omega cm$, mobility greater than $6000\,cm^{-2}/Vs$) (American Crystal Technologies) in a 9.4 T magnetic field at low temperature. The sample was placed in a continuous flow cryostat (Janis) and in good thermal contact with a sapphire wafer to facilitate heat dissipation (Fig. 3.7). Detection was preceded by the protocol $Sat - T_L - T_D - \pi/2$, where $T_L$ and $T_D$ indicate illumination and dark intervals, respectively. Saturation (*Sat*) prior to illumination was carried out via a string of $\pi/2$ pulses. The beam diameter was ~ 1.5mm.

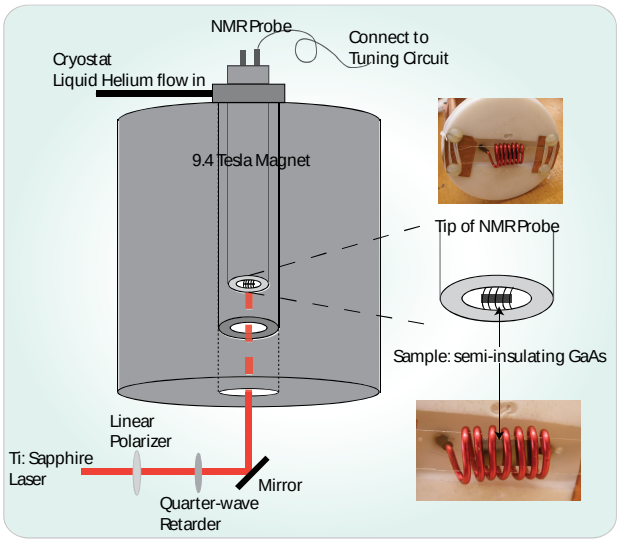


Fig. 3.7 OPNMR experimental setup of GaAs

The OPNMR signals of $^{71}$Ga as a function of light helicity were measured at two laser intensity regimes. In Fig. 3.8, the high intensity signal shows dependence on light helicity, in agreement to well-known results[17], the OPNMR signal is at the maximum when the quarter-wave plate sets the light to be right-/left- circularly polarized, and inverses the sign when passing from right-to-left or left-to-right circular polarization. At the lower intensity regime at this photon energy, the lack of response to the light helicity suggests a different mechanism.

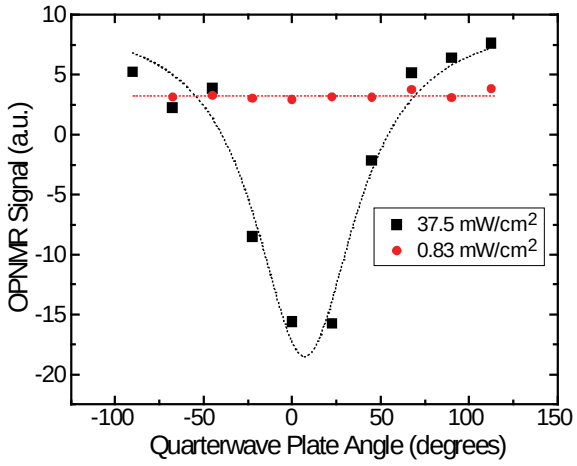


Fig. 3.8 OPNMR as a function of helicity for 71Ga

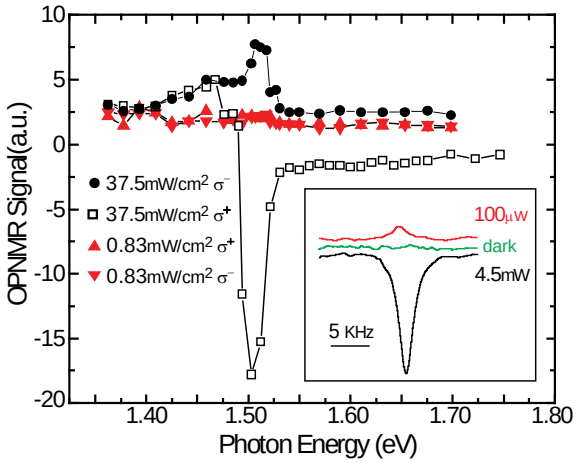


Fig. 3.9 OPNMR signal as a function of photon energy for 71Ga

Owing to signal-to-noise considerations, most studies have been conducted using strong illumination (5 mW and up, that is 37.5 mW/cm$^2$). In this regime, electrons (and thus nuclear) spins polarize in one direction or the other depending on light helicity. The excitation photon energy dependence of $^{71}$Ga NMR spectra which was measured over a wide range of photon energy scale (between 1.36 eV and 1.7 eV) at 8 K exhibits several defining characteristics in Fig. 3.9. Far above the band gap (1.52 eV), the sign of the OPNMR signal may be controlled with the light helicity and the spectrum exhibits oscillations as a function of photon energy due to the appearance of Landau levels.[37] Near the band gap, a maximum in the OPNMR signal is observed at 1.503eV (825nm), 20meV below the band gap due to the interplay of photon penetration depth and electron spin polarization[38]. Below the band gap, a different regime emerges where the OPNMR signal can no longer be controlled with light helicity and always presents a positive value with respect to thermal polarization. Previous studies have proposed mechanisms, perhaps involving an electronic species with a positive g-factor[12], but none have attempted to model this regime, nor have they provided experimental tests of these mechanisms.

The irradiation intensity dependent OPNMR for three nuclei ($^{71}$Ga, $^{69}$Ga, $^{75}$As) are displayed in Fig. 3.10 at the wavelength of 825nm (1.503 eV). The illumination time was 300 s. Previous literatures have reported the signal goes exponentially with light intensity positively or negatively, depending on the light helicity.[14] Our observation shows at the very low intensity the OPNMR signal increases positively as the intensity increases for all nuclei (inset, Fig. 3.10). The exponential increase at higher laser intensity has been reported before which is believed to be the increase of polarized nuclear at the localized shallow donor

sites.[1,21]

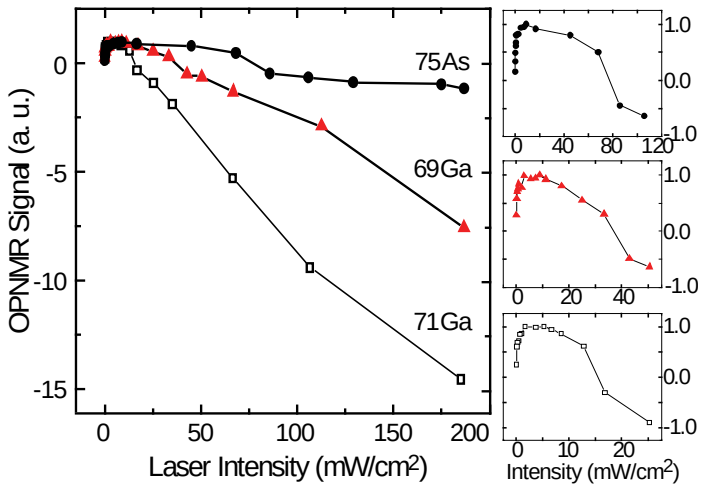


Fig. 3.10 OPNMR signal as a function of illumination intensity for all nuclei

The time dependence of OPNMR signals of $^{71}$Ga was measured within a time range up to 20 minutes (Fig. 3.11). The linear increase is observed both at high power and low power. The dark relaxation signal is included, showing a very tiny linear increase.

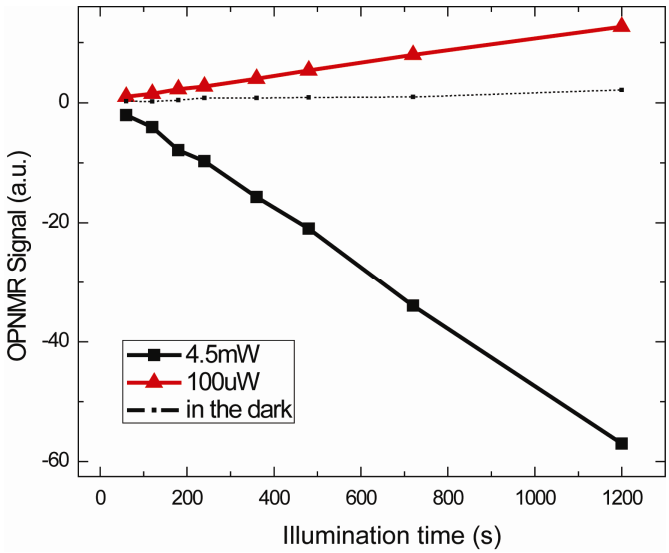


Fig. 3.11 OPNMR as a function of illumination time.

Finally, the temperature dependence of $^{71}$Ga OPNMR signals for $\sigma^+$ illumination was measured (Fig. 3.12). The optical enhancement decays as the lattice temperature increases

for high power. The low power signal and dark signal were measured at the same time. The little jump at 6 K and 7.8 K was due to experimental errors, caused by repeatedly lowing and raising the temperature.

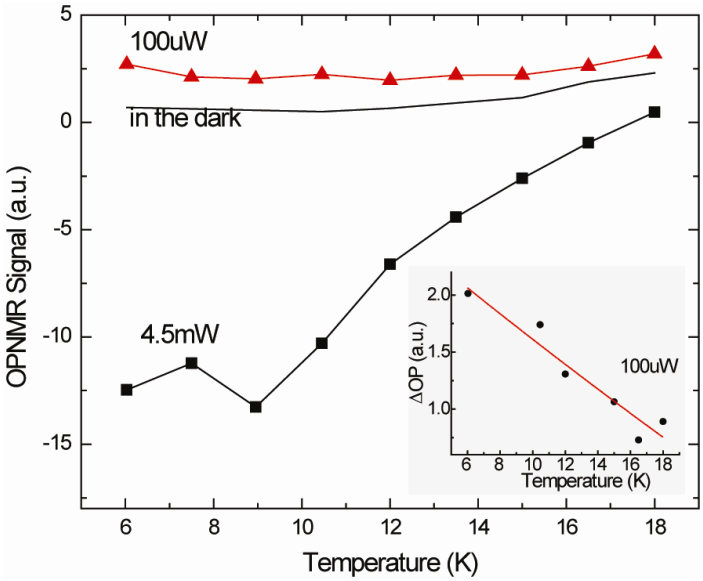


Fig. 3.12 OPNMR as a function of temperature

The process of optically polarizing bulk GaAs has been studied for many years. Previous model proposes that the spin-electrons are excited and spin exchange with electrons bound at shallow donors. Those bound spin-polarized electrons then polarize proximate nuclei primarily through the Fermi-contact hyperfine interaction.

To address the loss of sensitivity to light helicity in Fig. 3.8 and the always positive signal below the band gap in Fig. 3.9, a new model of polarization mechanism is proposed here. Previously, Paget and collaborators proposed a mechanism of light-induced quadrupolar relaxation.[39] This model was developed to explain the reduction of OPNMR signal by quadrupolar-induced depolarization, which is an effect of magnetic against an electric interaction effect. Here, we consider quadrupolar relaxation as a mechanism for polarization which, in certain regimes, may dominate over hyperfine polarization and reverse the sign of

the NMR signal. Quadrupolar relaxation occurs near shallow donors as the capture and release of electrons creates a fluctuating electric field gradient. These fluctuations are governed by the kinetic temperature of the electrons, and therefore drive the nuclear spins to this temperature, with no dependence on the electron spin polarization. The equilibrium spin temperature for nuclei under the quadrupolar interaction is always positive, and therefore results in a spin polarization which is positive with respect to the external field.

For the sake of simplicity, we ignore the thermodynamic nuclear and electronic magnetization and nuclear-spin-lattice relaxation. Hayes and others have showed the nuclear-spin-lattice relaxation in single-crystal semiconductors (undoped and compensated) can be neglected due to the very long nuclear spin life time at very low temperature[17]. In the standard description of OPNMR, the rate equation is given by

$$\frac{dI_z(r,\theta,t)}{dt} = -\frac{1}{T_{1H}(r,\theta)}(I_z(r,\theta,t) - I_{H,0}) - \frac{1}{T_{1Q}(r,\theta)}(I_z(r,\theta,t) - I_{Q,0}) + D\nabla^2 I_z(r,\theta,t) \quad , \quad (3\text{-}2)$$

where H and Q stand for hyperfine and quadrupolar relaxation, $I_{H,0}$ and $I_{Q,0}$ are the equilibrium values. The first two terms are from relaxation processes and the last term is from the spin diffusion. D is the diffusion coefficient[13,40,41,42,43].

The ratio of the two relaxation time scale $f$ is defined by, $f = \frac{T_{1Q}}{T_{1H}}$, where $T_{1H}$ and $T_{1Q}$ are hyperfine and quadrupolar relaxation time.

For a spin 3/2 system, the average expectation value of $I_z$ at thermal equilibrium is given by $< I_z >_{eq} = \frac{1}{2}\tanh(\Delta E / 2kT) + \tanh(\Delta E / kT)$. For $\Delta E << kT$, $< I_z >_{eq} = \frac{5}{4}\frac{\Delta E}{kT}$.

The steady-state value for hyperfine relaxation is $I_{H,0} = \frac{5}{4}\Delta S_z$, with $\Delta S_z = \frac{S_0 - S_{eq}}{1 + \tau / T_{1e}}$,

where $S_0 = \pm\frac{1}{4}$ is the polarization of electrons due to the light excitation, $S_{eq}$ is the thermal equilibrium polarization of electrons, $\tau$ is the recombination lifetime of electrons and $T_{1e}$ is the spin-lattice relaxation time of the electrons.

$S_{eq} = 1/2 tanh(-g\beta B_0 / 2kT)$

As shown in Appendix B, in the high magnetic field limit

$$\frac{1}{T_{1H}} = e^{-\frac{4r}{a_0}} \frac{1}{T_{1,0}} \tag{3-3}$$

$$\frac{1}{T_{1,0}} = \Gamma(\gamma_N b_e(r))^2 \frac{2\tau_H}{1+\omega_H{}^2\tau_H{}^2} e^4 \tag{3-4}$$

$$f = f_0 \frac{\Gamma}{1-\Gamma} F(r,\theta). \tag{3-5}$$

where $f_0$ is a constant which is a property of the nucleus under investigation, and $F(r,\theta)$ is the spatial term of radius and angle.

$$F(r,\theta) = \frac{1}{1+3\cos^2\theta} \frac{e^{-4(r/a_0-1)}}{[1-(1+\frac{2r}{a_0}+\frac{2r^2}{a_0{}^2})e^{-2r/a_0}]^2} (\frac{r}{a_0})^4.$$

Here, the idea of the light penetration depth is adopted. Therefore, $\Gamma(z)$, the donor occupation factor, is a function of depth, same as $P(z)$, the incident laser power. The total OPNMR signal is proportional to the integral (sum) of $I_z$ over $r$ and $\theta$. To predict the OPNMR signal, a relationship between $\Gamma(z)$ and $P(z)$ is needed.

We simulate $< I_z >$ in a simple three-dimensional cubic lattice with periodical boundary conditions. The nuclear spin system starts with zero-polarization.

In equation (3-5), $f_0$ is a fitting parameter, $f_0 \propto \frac{\gamma^2}{R_{14}{}^2 Q^2}$. It is difficult to determine how much laser power enters the sample due to scattering off optics and reflection at the wafer surface. And it is impractical to use a standard for absolute determination of $< I_z >$ due to

very long relaxation times, so the OPNMR signal is presented in arbitrary unites. Also, the sensitivity of the NMR probe changes with temperature, so room temperature signals do not provide an accurate standard.

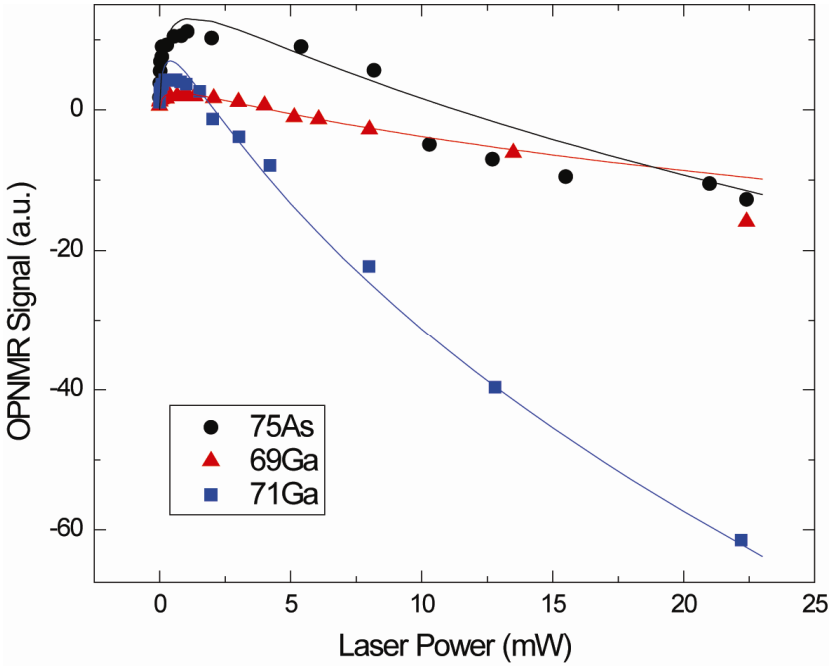


Fig. 3.13 Theoretical Predictions for OPNMR signal overlaid in data for three nuclei: $^{75}$As (black), $^{69}$Ga (red), $^{71}$Ga (green).

As seen in Fig. 3.13, when applied to the case of laser with $\sigma^+$ illumination and short irradiation times, the model accurately predicts the magnitude of the OPNMR signal vs. power curve, including the crossover between the helicity-independent quadrupolar dominated regime to the helicity dependent hyperfine dominated regime as intensity increases. The continued signal growth at higher powers, beyond the point where $\Gamma$ has reached is maximum value, indicates a high-magnetic field regime where $1/T_{1,H}$ scales with the free electron concentration. By adjusting the value of $f_0$, we obtain fits from each nucleus in the same sample: $^{71}$Ga, $^{69}$Ga, and $^{75}$As (Fig. 3.10). These curves exhibit the correct trend where the larger product of quadrupolar moment $Q$ and electrostatic anti-shielding

$R_{14}$ ($^{75}$As>$^{69}$Ga>$^{71}$Ga) and smaller magnetic moment (magnetogyric ratio $\gamma_N$ ) ($^{75}$As<$^{69}$Ga<$^{71}$Ga) results in the crossover being shifted to higher laser intensity in the order of $^{71}$Ga<$^{69}$Ga<$^{75}$As.

(2) Optical Patterning of Nuclear Polarization

Spatial control of nuclear polarization has many applications, e.g., separately tuning the resonance conditions for arrays of confined electrons. These effects have been shown to perform coherent spin rotations of shifting electrons.[44] Current methods for patterning nuclear polarization are limited by the need of ferromagnets, lithographic printing techniques, or high-filed gradients.[45] Here, we demonstrate a three dimensional patterns of positive and negative nuclear magnetization with all-optical method.

Our model which combined the hyperfine and quadrupolar interactions predicts that not only can the magnitude of $< I_z >$ vary throughout the depth of the sample, but the sign of $< I_z >$ may vary as well. Qualitatively, for high laser power and near to above gap irradiation, the majority of the light is absorbed near the surface of the sample, with a high donor occupation fraction and free electron concentration, $\Gamma$ is close to 1, $f$ is large. The OPNMR signal is then almost entirely due to this region where hyperfine relaxation is dominant (Fig. 3.14a). As the photon energy is lowered well below the band gap, the penetration depth becomes large and the rate of absorption per unit volume is much lower, and is spread throughout a larger region of the sample. In this case, the OPNMR signal is due to a large region of the sample with lower donor occupation fraction and free electron concentration where quadrupolar relaxation dominates (Fig. 3.14b). For near and above gap irradiation, the OPNMR signal will always be limited to the region near the surface due to small penetration depths. However, by reducing the laser power, the free electron concentration and donor occupation fraction in this region may be lowered so that

quadrupolar relaxation dominates (Fig. 3.14c). Clearly there also exists an intermediate case for both laser power and photon energy where the net OPNMR signal is zero. This model predicts that in this case $< I_z >$ is not zero throughout the sample, but rather there are regions of positive and negative $< I_z >$ (Fig. 3.14d).

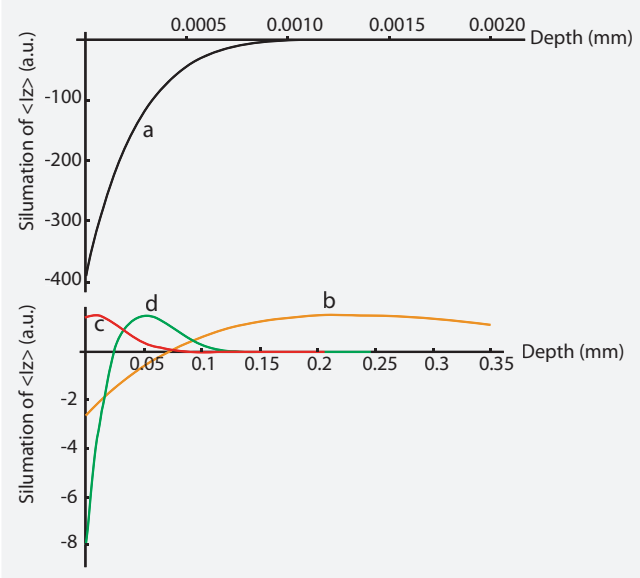


Fig. 3.14 Prediction of $< I_z >$ as a function of depth for 0.4mm thick GaAs wafer with irradiation at a)1.52eV high power, b)1.48eV high power, c)1.503eV low power, and d)1.503eV intermediate power

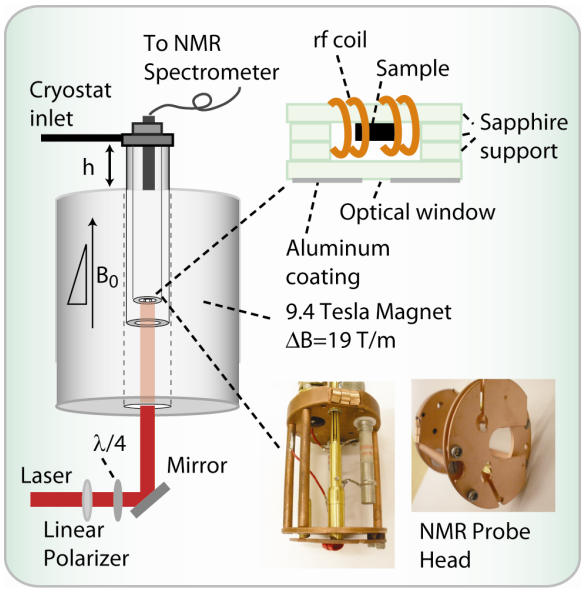


Fig. 3.15 Stray-Field-Imaging experimental setup.

We employ the Stray-Field Imaging (STRAFI) technique[17], which makes use of the gradients in the stray field of the 9.4 T magnet, at the temperature of 6.5 K, unless otherwise noted. The schematic experimental setup is shown in Fig. 3.15a.

To ensure good thermal conductivity, we use Apiezon N grease to mount the sample of thickness 350 $\mu m$ atop a long, rectangular sapphire strip. The strip bridges the opposite sides of a 3 cm diameter opening at the center of a thin copper plate, whose orientation relative to the static magnetic field can be slightly adjusted using screws connected to the outside of the cryostat via long G10 rods. A split-coil surrounding the sample (and sapphire wafer) as part of a purpose-made cryogenic probe serves as the radio-frequency source. The coil shape and size are chosen so as to optimize the sample filling-factor while avoiding making physical contact with the support wafer or GaAs crystal. As shown in Fig. 3.15, the area illuminated by the laser beam on the sample surface is defined by a proximal 1x1 $mm^2$ square window etched on an aluminum-coated sapphire strip aligned to coincide with the coil central gap. We use an optical expander to widen the laser beam so as to reach a 5-mm-diameter waist before the aluminum window, thus ensuring homogeneous intensity over the optically pumped surface. We control the beam helicity using a linear polarizer and a quarter wave plate. We illuminate the sample at 6.5 K through the quartz windows at the bottom of a modified cryostat (Janis-Varitran), and use the G10 rods protruding at the upper end of our NMR probe to align the GaAs wafer perpendicular to the direction of the static magnetic field. To accomplish this, we adjust the copper plate orientation while monitoring the part of the laser beam reflected from the aluminum-coated sapphire; this method allows us to reach a sample orientation precision better than half a degree. In preparation for the

optical-pumping experiments reported herein, we conducted extensive preliminary experiments aimed at determining the magnetic field gradient as a function of the sample position within the magnet bore. For this purpose, we recorded the $^{71}$Ga NMR signal from the GaAs wafer at room temperature for multiple displacements of the cryostat from its rest position atop the magnet. NMR spectra were attained using a simple excitation-acquisition protocol with 1-$\mu s$-long RF pulses so as to ensure the broadest excitation bandwidth possible. The magnetic field gradient is linear over the sample volume and exceeds 70 T/m at the maximum displacements we tested. For the present optical pumping experiments, we use a somewhat moderate gradient (19 T/m) as a reasonable tradeoff between spatial resolution and signal-to-noise ratio for typical illumination times (10 min).

With a natural NMR linewidth of approximately 4kHz for 69Ga and a gradient of approximately 19T/m, we achieved spatial resolution in the z-direction of 20 microns. As shown in Fig. 3.15b, data are acquired by first saturating the spin transitions with a series of RF pulses, after which the sample is illuminated with circularly polarized near-gap irradiation followed by signal acquisition via a $\pi/2$ pulse and inductive detection of the transverse magnetization.

The STRAFI data in Fig. 3.16 correspond directly to the sign and magnitude of nuclear polarization as a function of depth in the sample. At the lowest illumination intensity (4mW/cm$^2$), the polarization is positive throughout the sample, and is nearly independent of helicity, consistent with the bulk experiments[15] reported previously. At the highest illumination intensity (102 mW/cm$^2$) the sign of the polarization throughout much of the sample may be controlled with light polarization, consistent with many previous bulk studies

in this regime.[14,46] Here, the intermediate regime is of interest. In this regime of intermediate

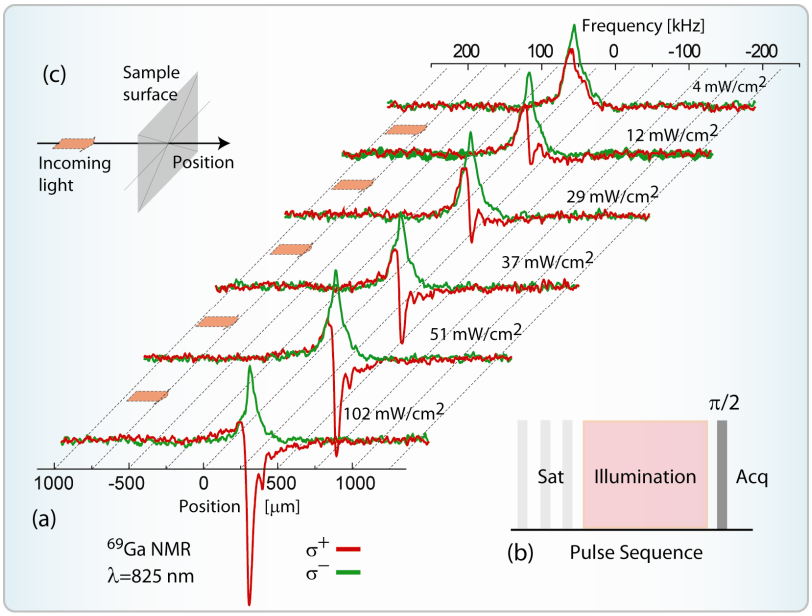


Fig. 3.16 (a) Spatial patterns of nuclear polarization for different laser intensities. (b) RF pulse sequence. (c) Incoming light illuminates the sample from the left (coincident with higher frequencies in the setup, see upper horizontal axis.) The origin is chosen to approximately coincide with the GaAs wafer surface.

illumination intensity, using $\sigma^+$ polarization, regions of opposite spin polarization are created within close proximity in the GaAs wafer. A negative signal is found closer to the surface of the sample where absorption is greatest and electron spin-exchange dominates the nuclear polarization process. A positive signal emanates from that portion of the wafer where the light intensity has decayed. In these regions of reduced absorption, the donor occupation fraction decreases such that the quadrupolar polarization mechanism is dominant. By adjusting the wavelength of light (Fig. 3.17), we vary the optical penetration depth, controlling the length scale of the patterns of polarization. For example, for irradiation at 810

nm, our analysis reveals that we created features approximately 40 microns wide.

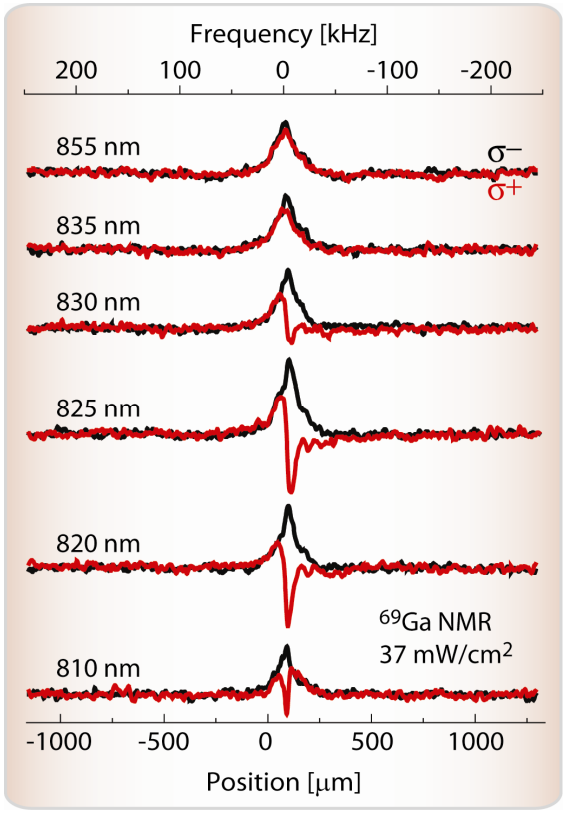


Fig. 3.17 Stray Field Imaging of nuclear polarization for $^{69}$Ga as a function of irradiation wavelength after an irradiation of 10 min. Red curves correspond to $\sigma^+$ helicity and black curves correspond to $\sigma^-$. Decreasing the wavelength to 810 nm creates features approximately 40 microns in length.

Without detailed knowledge of the electron recombination dynamics, optical absorption at high-field and low temperature, and kinetics of electron capture at donors, it is difficult to quantitatively model the dependence of the patterns on illumination wavelength and intensity. However, assuming a single binary recombination mechanism and Langmurian binding of free electrons to donors, combined with literature values for optical absorption[34], we reproduce the shape of the STRAFI images as a function of illumination intensity for a given

wavelength (Fig. 3.18). We also note that for most experimental conditions there is a region of positive polarization localized at the irradiated surface. We attribute this to a depletion layer of low donor occupation near the surface. Briefly, defect states pin the Fermi-level mid gap at the surface and an electric field extends from the surface into the bulk. Shallow donors may be ionized in the regions where the electric field exceeds about 5000 V/cm.[47] The approximate width of the depletion layer is given by48: $L = (\frac{2\varepsilon\varepsilon_0\phi_0}{\rho})^{1/2}$,

where $\varepsilon$ is the dielectric constant, $\varepsilon_0$ is the vacuum permittivity, $\phi_0$ is the potential of the pinned Fermi-level at the surface, and $\rho$ is the charge carrier density. In order to theoretically reproduce STRAFI images, a depletion layer of $50\,\mu m$ was included in the simulations.

Assuming the Fermi-level is pinned mid-gap, this corresponds to a carrier concentration of ~1014 $cm^{-3}$, which is similar to the free electron concentrations predicted by the simplified model for a semi-insulating sample at low temperature with optical illumination. Given this very simplistic model, the agreement with experiment (Fig. 3.18) is nearly quantitative.

We also investigated the isotope dependence of the patterning process (Fig. 3.18). As expected, the isotope with the larger quadrupole moment and smaller gyromagnetic ratio required greater irradiation intensity to transition from positive to negative polarization. Comparing the intermediate irradiation intensity data in Fig. 3.18 (for example 14 $mW/cm^2$), we observed the unique situation where different isotopes of the same chemical species have opposite polarization at the same location in the sample, suggesting the ability to create hetero-nuclear spin order via dipolar or indirect J-coupling.[49]

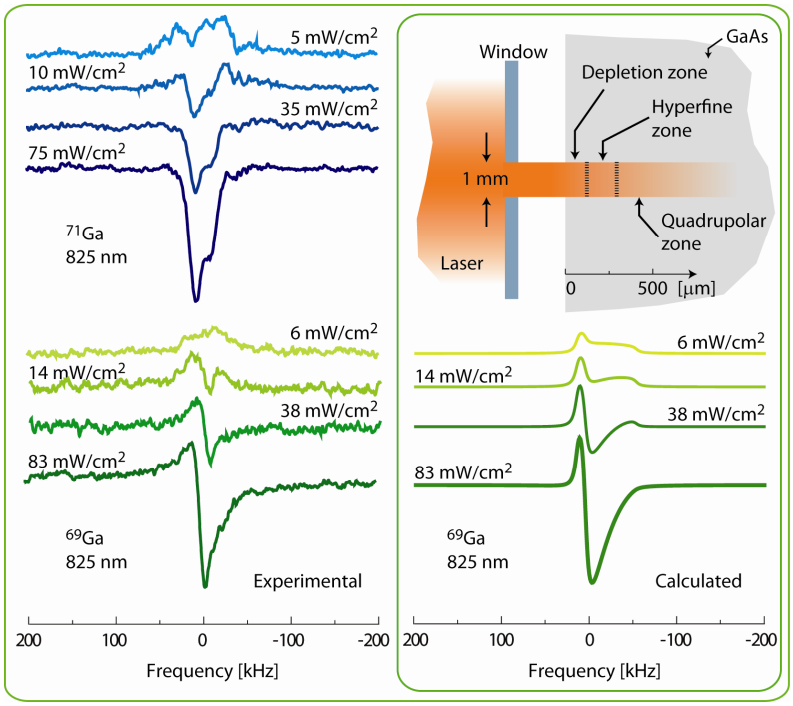


Fig. 3.18 Stray Field Images of nuclear polarization of $^{71}$Ga and $^{69}$Ga. The isotope with larger quadrupolar moment and smaller magnetic moment, transitions from the negative hyperfine regime to the positive quadrupolar regime at higher irradiation intensity. Simulated STRAFI images for $^{69}$Ga capture the changing shape of the distribution of nuclear polarization with illumination intensity.

Optical pumping can be combined with NMR pulse sequences to further control nuclear polarization. As a proof of principle, we combined periods of optical pumping of varied intensity and wavelength with NMR $\pi$ pulses to isolate regions of hyperfine- and quadrupolar-induced polarization (Fig. 3.19). Many sophisticated NMR pulse sequences exist that interconvert various types of spin order and coherence, which may be combined with spatially-patterned polarization to create a range of spatially-dependent spin dynamics.

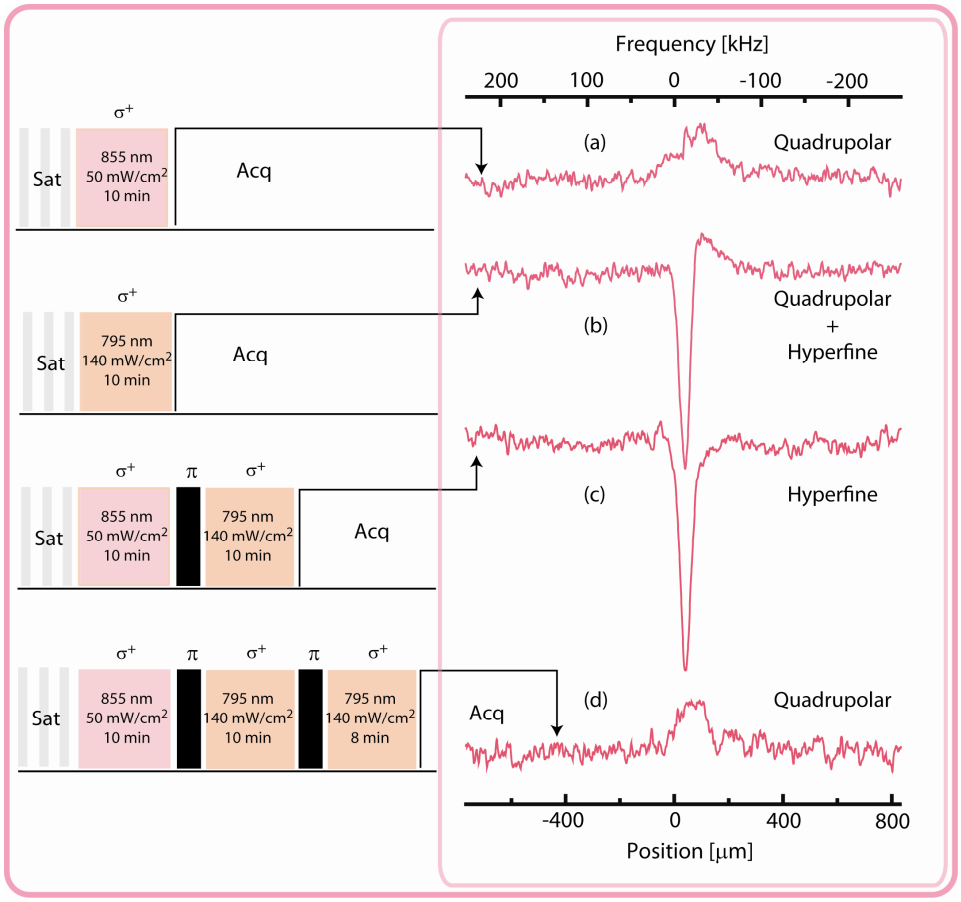


Fig. 3.19 Optical pumping parameters may be chosen so that (a) quadrupolar relaxation dominates, or (b) both mechanism act simultaneously on different regions in a sample. By combing periods of optical pumping with different intensity and wavelength, separated by $\pi$ pulses, only (c) the hyperfine or (d) quadrupolar polarization remain.

(3) Spin diffusion and Saturation of polarization

The light excitation leads to polarization of those nuclear spins that are in the vicinity of localized defects, described by the first two terms in equation (3-2), as a source term. The third term acts as a source of polarization for remote nuclear spins which are not directly contact with the localized electrons. The evolution of nuclear magnetization in GaAs is believed to (1) have fast relaxations by the electrons trapped at the donor centers, up to a distance from the donor site equal to the diffusion radius $\delta$, where the evolution of the nuclear magnetization by spin diffusion is negligible; (2) beyond $\delta$, the spin diffusion plays a dominant role and the magnetization is homogeneous and increase in a time of order of the bulk nuclear relaxation time. [13,37,38,39,40] In literature, the diffusion radius $\delta$ is larger than the Bohr radius $a_0$ [36], where $a_0$ is the electron Bohr radius, in the order of 100 $\overset{o}{A}$ in bulk GaAs.

Using $10^{-13}$ $cm^2/s$ as the value of diffusion constant D, we run a simulation of $< I_z >$ as a function of time for $^{71}Ga$ (Fig. 3.20) which shows a very similar trend (of OPNMR signal vs. $\tau_L$) as Fig. 3.11.

Previous experiments of evidence of spin diffusion were done by switching off the light excitation and measuring the characteristic time of the resulting decay of the nuclear field.[37] However, the simulation shows that if the polarization is easily saturated in the vicinity of localized donor center, while spin diffusion assists the polarization to spread out more efficiently, an enhanced polarization can be accumulated via tens of hundred repetitions of "illumination-diffusion" cycles. This is a direct evidence of the existence of spin diffusion within the range of the diffusion radius.

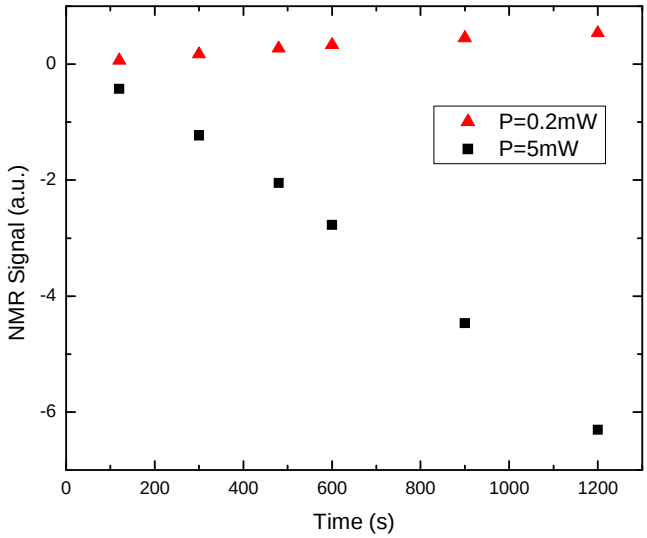


Fig. 3.20. Simulation of OPNMR signal vs. illumination time for $^{71}$Ga.

We detected the $^{71}$Ga and $^{69}$Ga OPNMR signal with the aforementioned basic optical pumping experimental setup, in a 9.4 T magnet, at 6.2 K (Fig. 3.7). The semi-insulating GaAs crystal was mounted on a sapphire wafer, which sit on the cold finger of the Janis cryostat. The pulse sequence is $Sat - T_L - T_D - \pi/2$ (Fig. 3.21). The Saturation $Sat$ is a string of $\pi/2$ pulses, followed by illumination time $T_L$ and dark time $T_D$. And in the following experiments, $T_L$ and $T_D$ may be fractioned into $N_L$ intervals, i.e., $T_L = N_L \times t_L$ and $T_D = N_L \times t_D$. After repeating a multiple intervals of "light-dark", the final acquisition is conducted after a $\pi/2$ pulse. The $t_L$ and $t_D$ were set by a shutter which received the TTL signals from the spectrometer.

First of all, it is necessary to recognize and rule out the effect of relaxation in the dark. In Fig. 3.21 a, as dark time $T_D$ increases, the signal from dark relaxation becomes stronger. We can see in Fig. 3.21 b that for the hyperfine dominated polarization with $\sigma^+$ optical

pumping at high intensity (183mW/cm$^2$) of light excitation, the dark relaxation does not change the line shapes, but for the illumination at 86mW/cm$^2$, the dark relaxation changes the line shape. To exclude the impact of the relaxation in the dark, we acquired the spectrum A ($T_L = 30s$ , $T_D = 0$ ) and B ($T_L = 0, T_D = 300s$ ), and got the addition of each point of A and B which was spectrum C (C=A+B). We find that the line shape of C is equivalent to experimental spectra D, which was for $T_L = 30s$ and $T_D = 300s$ (Fig. 3.21 c). So we claim that what we observed is irrelevant to dark relaxation. In absence of light illumination, the evolution of nuclear spin system is completely governed by spin diffusion. Although the total bulk average magnetization remains unchanged, the transfer of magnetization by spin diffusion modifies the polarization experienced by optical pumping.

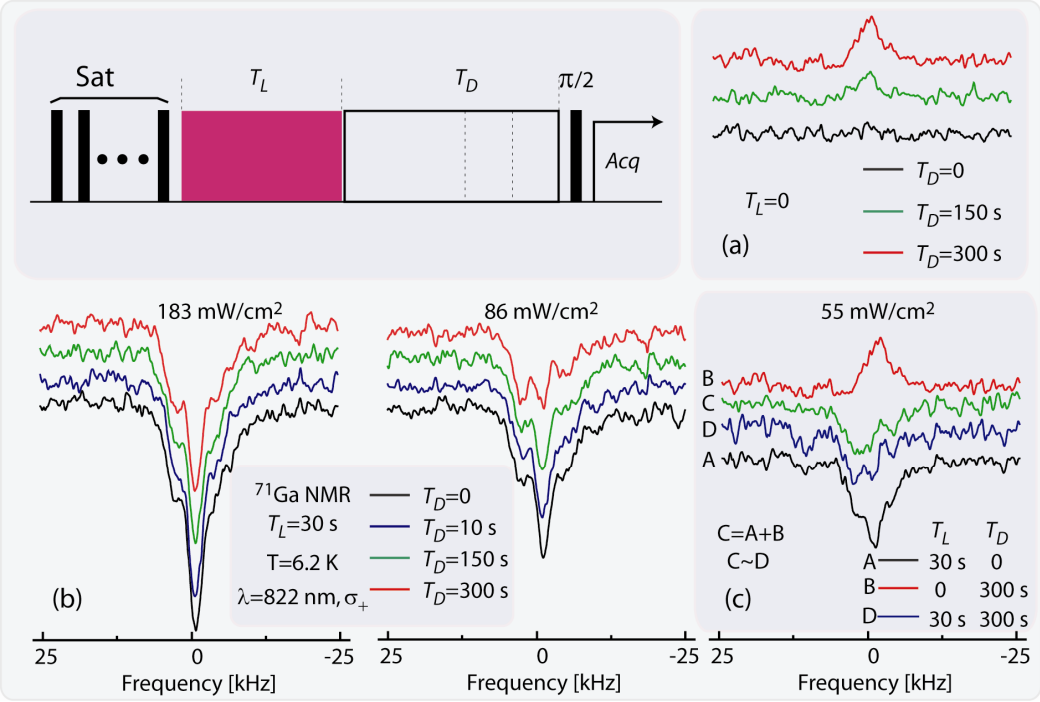


Fig. 3.21 $^{71}$Ga OPNMR spectrum. The RF pulse sequence is shown on the upper left. The total dark time is varied on the lower left. And the pure “dark spectra” are sown on lower right.

In previous OPNMR experiments, samples were exposed to light for a continuous protocol as a relative long $T_L$ (usually a few minutes) followed by a short $T_D$ (or $T_D = 0$), the effect of diffusion was not strongly supported. However, by extending $T_D$ and dividing the continuous protocol into many cycles, we are able to see the effect of diffusion. In our experiment, we fix the total illumination time $T_L$ and dark time $T_D$. By increasing the number of the cycles $N_L$, we reduce the pumping time $t_L$ for each cycle, so that the OP polarization built from whatever mechanism is small enough and can be redistributed by diffusion process during $t_D$, while total bulk-average polarization does not change. Thus, for every $t_L - t_D$ cycle, the optical pumping builds up and diffuses to distant nuclei. In this way of pumping and diffusion cycles, we note that the quadrupolar effect is most affected.

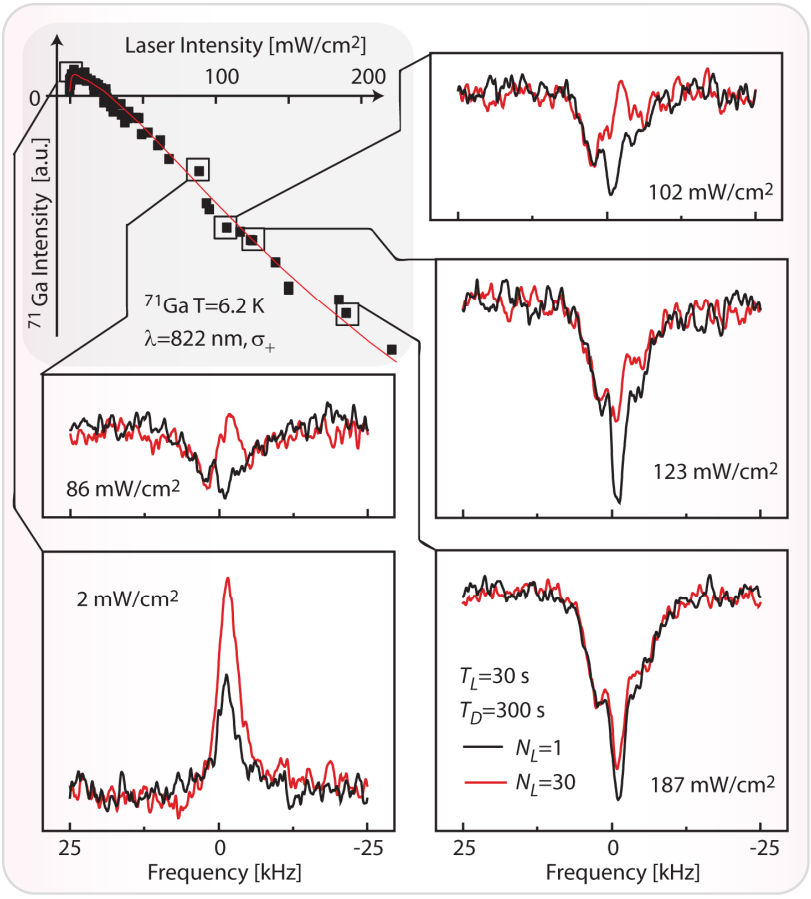


Fig. 3.22 $^{71}$Ga NMR Spectrum at different laser intensity for $N_L = 1$ and $N_L = 30$.

In Fig. 3.22, we present five sets of $^{71}$Ga NMR spectrum at featured illumination intensities chosen from the curve of magnetization as a function of laser intensity, whose total magnetization is represented by the black spectrum. The curve of magnetization as a function of laser intensity has been reported in Fig. 3.10. In the regime of strong illumination, the hyperfine mechanism dominates and gives negative amplitude, and in the regime of weak illumination the quadrupolar dominates and gives relatively small positive amplitude.[15] The total illumination time $T_L$ and dark time $T_D$ are kept as 30s and 300s, respectively. Thus, the contribution from dark relaxation for every curve is equivalent and can be just ignored. In the high power regime (187 mW/cm$^2$), the fraction of $T_L$ and $T_D$ plays no role; in the intermediate regime (123 mW/cm$^2$, 102 mW/cm$^2$, and 86 mW/cm$^2$), the influence of 30

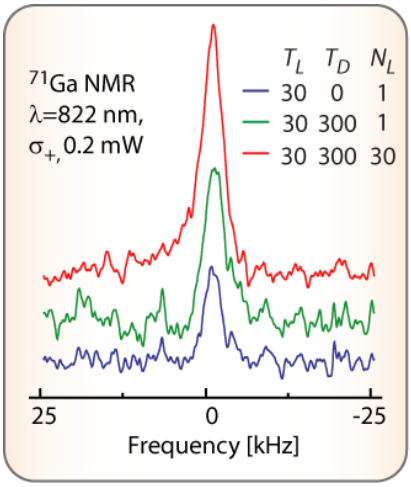


Fig. 3.23 A set of $^{71}$Ga NMR spectra. The pure optical pumping spectrum is shown in blue.

repetitions raises up the central hyperfine peak or even flip it from negative to positive, due to the strengthen of the quadrupolar effect. In the lowest power regime (2 mW/cm$^2$), where the quadrupolar completely dominates, the repetition further enhances the positive peak. A

reference of the pure effect of 30 s pumping is added in Fig. 3.23 as the blue curve. The dark relaxation always drives the nuclear spin to a positive spin temperature, due to the thermal equilibrium with the lattice.

In Fig. 3.24, a series of $^{71}$Ga NMR spectra for illumination of $\sigma^+$ at 55 mW/cm$^2$ is displayed. The left spectra were directly obtained from acquisition, while the right ones were subtracted the dark relaxation from the left. The "Ref" spectra were the acquisitions after $T_L$ without waiting in the dark. And for all others, the total illumination time and dark time were kept as constant. At this intensity, the hyperfine feature is displayed in the Refs. For a fixed ratio of $T_L / T_D$, as $N_L$ increases, quadrupolar effect is enhanced. At $N_L = 1$, the spectra are similar to the Refs, showing the hyperfine feature. At $N_L = 30$, the central peaks of transition almost become positive. Finally, at $N_L = 1500$, they are completely dominate by quadrupolar effect, leaving no evidence of hyperfine relaxation. And for a fixed number of repetitions, the amplitude of $T_D = 300s$ is much lager than that of $T_D = 150s$. This indicates that longer waiting time in dark means more effectively redistribution of polarization, so that the quadrupolar interaction can build up more magnetization in each cycle.

The isotope $^{69}$Ga has been investigated at 120 mW/cm$^2$ in Fig. 3.25. The spectrum for $N_L = 1$ is the same as the Ref, where the hyperfine relaxation is dominant and the OP signal is negative. An obvious transition happens when $N_L = 300$, i.e., $t_L = 0.1s$ and $t_D = 0.5s$, the hyperfine signal is tampered dramatically. At $N_L = 6000$, i.e., $t_L = 0.005s$ and $t_D = 0.025s$, the hyperfine effect is eased up completely, leaving a huge quadrupolar effect. The one by one comparison between $^{71}$Ga and $^{69}$Ga at the same light intensity is in Fig. 3.26. Due to the larger quadrupole moment and smaller gyromagnetic ratio of $^{69}$Ga, at 55 mW/cm$^2$

it shows a more positive signal while $^{71}$Ga is at zero-crossing (black). The diffusion plays an

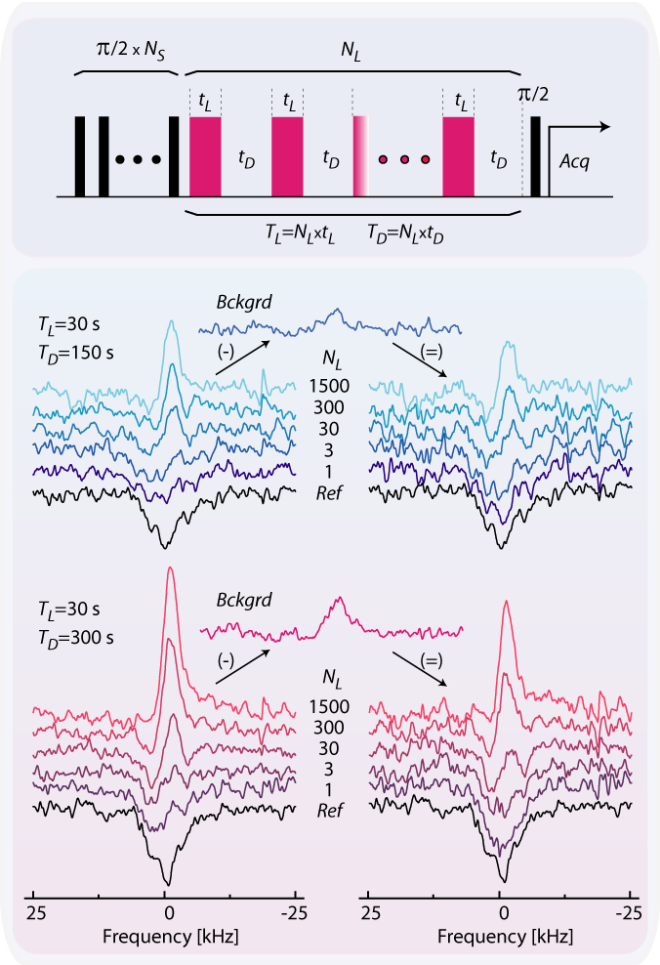


Fig. 3.24 $^{71}$Ga NMR spectra for illumination of $\sigma^{+}$ at 55 mW/cm$^2$. For Bckgrd, $T_L = 0$ and $T_D = 150s$ (top) and 300 s (bottom). For Ref $T_L = 30s$ and $T_D = 0$.

important role such that a significant increase in quadrupolar way exhibits in $^{69}$Ga by means of fraction the illumination and dark time. At 150 mW/cm$^2$, the fraction does not modify the line shape by a huge amount. However, by comparing with $^{71}$Ga, $^{69}$Ga still shows a bigger change due to its lager quadrupole moment.

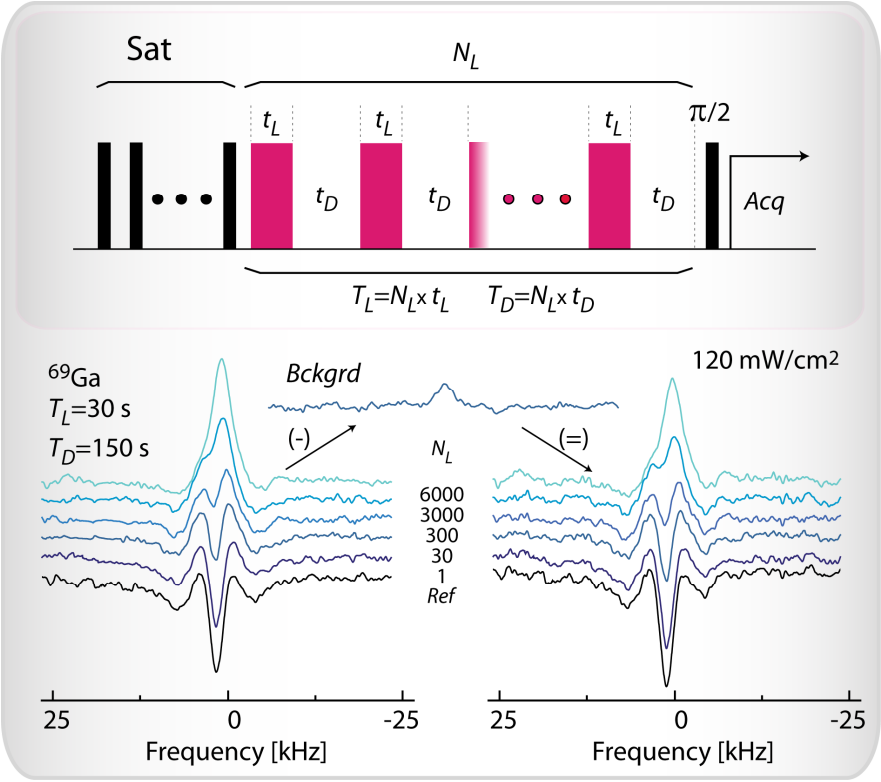


Fig. 3.25 $^{69}$Ga NMR spectra for $\sigma^+$ at 120 mW/cm$^2$. For Bckgrd $T_L = 0$ and $T_D = 150s$. For Ref $T_L = 30s$ and $T_D = 0$.

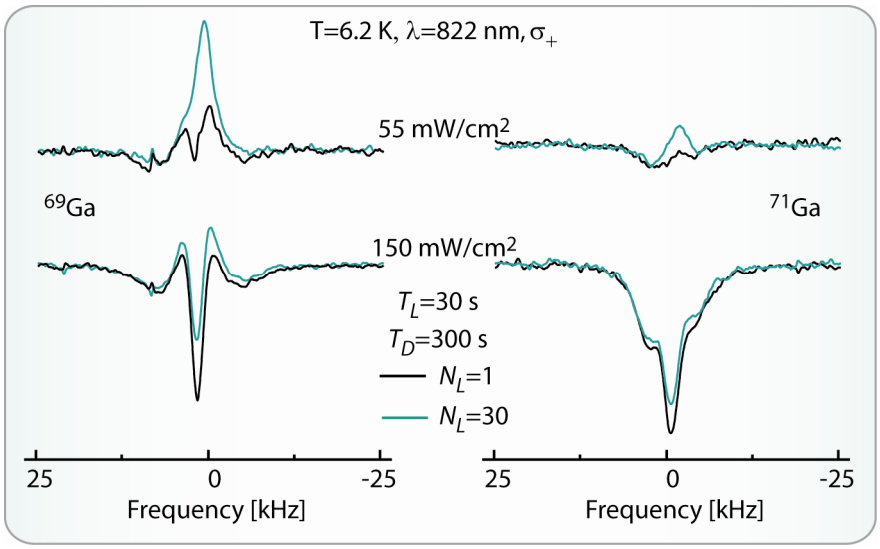


Fig. 3.26 NMR spectra for $^{69}$Ga and $^{71}$Ga. $^{69}$Ga shows an enhanced quadrupolar effect with multiple repetitions at 55 mW/cm$^2$ than $^{71}$Ga.

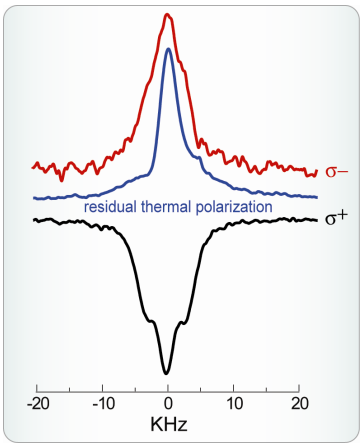


Fig. 3.27 A comparison between thermal polarization and optical pumping with quadrupolar splitting.

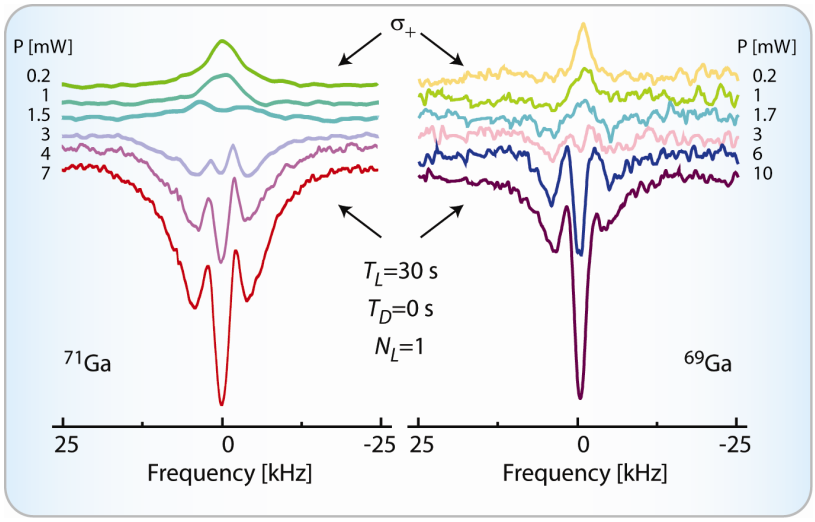


Fig. 3.28 The NMR spectra of $^{71}$Ga and $^{69}$Ga as a function of light power. The strain-induced quadrupolar splitting of $^{71}$Ga is stronger than that of $^{69}$Ga.

As may be noticed, some spectra shown with hyperfine interaction exhibit the quadrupolar splitting. We claim that it is due to the stain induced by tiny grease drops on the sample surface. In Fig. 3.27, we present the optically pumped signals, together with the residual thermal polarization, which was acquired right after when the liquid helium temperature was

reached before any light exposure. At room temperature, there is no strain induced by grease, so the blue spectrum shows no quadrupolar splitting. An interesting comparison of quadrupolar splitting between the two isotopes in Fig. 3.28 shows clearly that the splitting of $^{71}$Ga is always stronger that that of $^{69}$Ga. As the light intensity goes down and quadrupolar interaction dominates, the splitting disappears. Since the origin of the quadrupolar splitting is out of scope of this paper, we simply claim that the quadrupolar splitting is caused by grease induced strain.

An important tendency of $^{69}$Ga central peak amplitude as a function of each diffusion time $t_D$ is shown in Fig. 3.29. In this experiment, the overall illumination time was always fixed as 30 s. For shorter illumination time $t_L$, the repetition number was bigger, so that the overall dark time was longer, e.g., for $t_L = 5ms$ the repetition number equals 6000, and the total dark time $T_D = 6000 \times t_D$. The curves with dotes are experimental readout, and the ones without dots are processed as the doted values subtracted the dark relaxation values. We chose the light intensity as 120 mW/cm$^2$, so that the central peak amplitude for $t_L = 50ms$ was negative, which is a typically hyperfine dominant. The central peak amplitude almost goes linearly with $t_D$, which means the quadrupolar polarization dominates and beats off hyperfine relaxation. However, the curvature for $t_L = 5ms$ indicates two things that (1) the polarization is not saturated in this region, (2) although the polarization is so little in 5 ms, by increasing $t_D$ the diffusion moves away more polarization near the localized donor center, then ultimately the maximum polarization by quadrupolar relaxation will be reached. In another word, the curve will asymptotically reach a value which is the maximum

polarization by quadrupolar interaction, because for a certain $t_D$ the diffusion rate is optimum so that the polarization near the donor site will be totally transferred away, and by further increasing the $t_D$ the total polarization will not increase. 5 ms is at the limit resolution of the shutter in our setup. We believe with a shutter in higher resolution, one can see the asymptotic trend achieved and get an estimation of the diffusion constant.

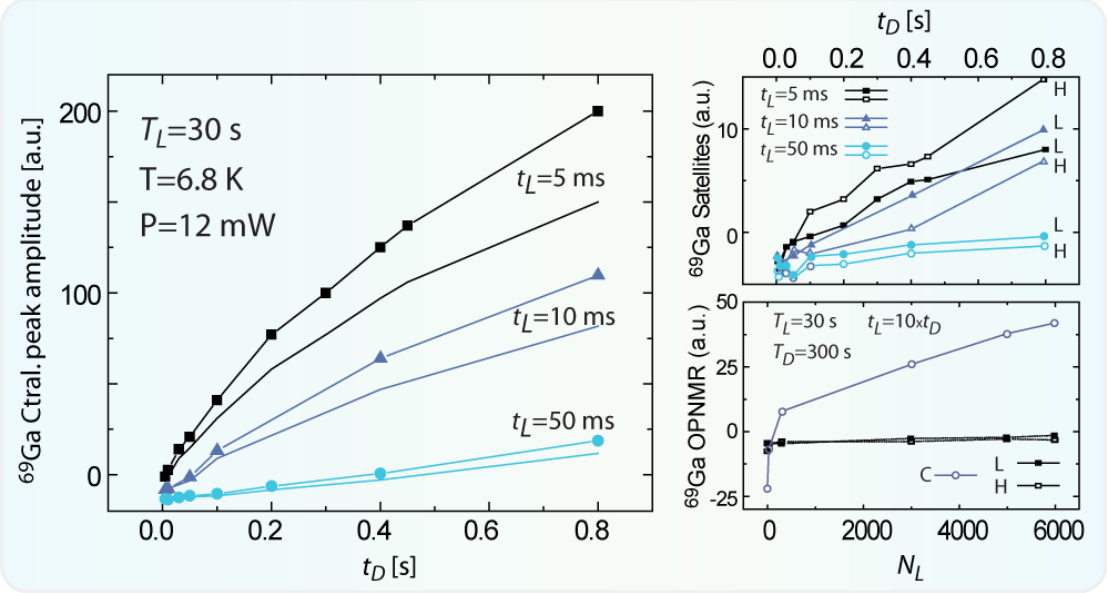


Fig. 3.29 $^{69}$Ga central peak amplitude as a function of dark time.

Considering that the rates of hyperfine and quadrupolar relaxation are both functions of distance from a give donor site, this suggests the possibility of achieving nuclear spin polarization on a similar scale to the Bohr radius (~ 10 nm in GaAs), which can be applied to the spin-based quantum computing devises.

## IV. Summary

In this work, we have presented some features of dynamic nuclear spin polarization on GaAs. We recall that the experimental methods presented here is very general. The time-resolved optical Faraday rotation has been applied to observe the electron spin precession under nuclear spin field, with high sensitivity and spatial resolution. And the optically-pumped nuclear magnetization has been measured via pulsed-NMR. Based on the measurements of OPNMR on GaAs, we have observed that at low illumination intensity the OPNMR signal is independent of light helicity and photon energy. We have developed a new model of nuclear spin polarization process, which combines hyperfine relaxation and quadrupolar relaxation. We have demonstrated this low intensity OPNMR signal is due to quadrupolar effect. And the transition from quadrupolar-dominated to hyperfine-dominated behavior occurring at increasing values of laser intensity in the correct order is supporting our model. By harnessing the different dependence on magnitude and sign of OPNMR signal through the depth of the sample at different illumination condition, we have demonstrated an all-optical creation of three-dimensional patterning of nuclear spin polarization in micron scale via stray-field imaging method. Such nuclear spin fields can be applied to tune the resonance frequency of confined spins, giving a new degree of freedom in spintronic device architectures with optical and electrical controls. Finally, a demonstration of nuclear spin polarization in nano scale via diffusion has been made, providing a depth understanding for the process of nuclear spin polarization by optical pumping. The nano scale inhomogeneity in semiconductor also provides a potential tool in quantum information technology.

Appendix

A: Optical Faraday Rotation in Voigt geometry

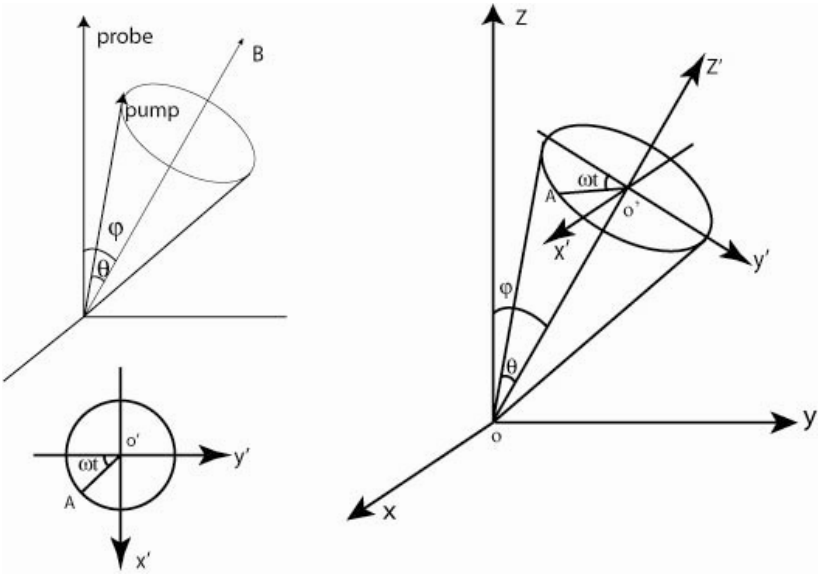


The optical pumping is along the Z' while the probe is in the direct of Z, the angle in between is $\varphi$. To get the projection of OA on the Z, it is clear to do a coordinate transformation from X'Y'Z' to XYZ.

$$x = A^{-1}x', \tag{A1}$$

where the corresponding Euler Angle is $(0, -\varphi, 0)$.

Assuming the length of OA is 1, we can get

$$x = \begin{bmatrix} \sin\theta\sin\omega t \\ -\sin\theta\cos\omega t \\ 0 \end{bmatrix}, \tag{A2}$$

$$\text{and} \quad A^{-1} = \begin{bmatrix} 1 & 0 & 0 \\ 0 & \cos\varphi & \sin\varphi \\ 0 & -\sin\varphi & \cos\varphi \end{bmatrix}. \tag{A3}$$

$$\text{So that} \quad x = A^{-1}x' = \begin{bmatrix} \sin\theta\sin\omega t \\ -\cos\varphi\sin\theta\cos\omega t \\ \sin\varphi\sin\theta\cos\omega t \end{bmatrix}. \tag{A4}$$

The total projection of OA along the Z axis is $\cos\theta\cos\varphi+\sin\varphi\sin\theta\cos\omega t$ .

We tested time-resolved Kerr rotation in Voigt geometry on CdTe at room temperature (Fig. A1). Due to the qualitative large value of electron g-factor (-1.27) we see spin precession in a short time delay. This was the first trial for the understanding of Voigt geometry.

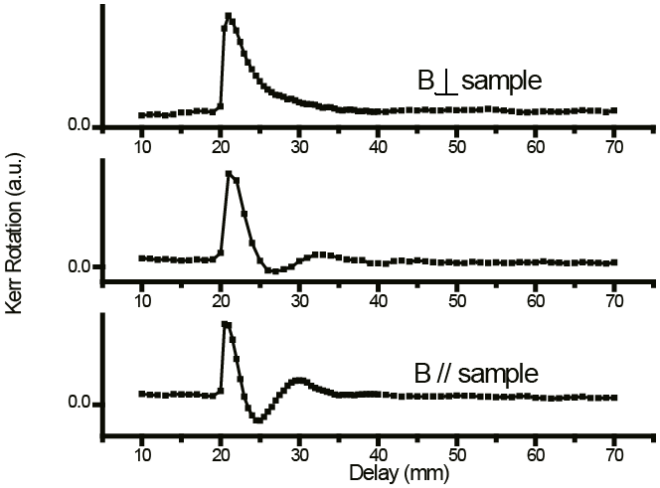


Fig. A1 Voigt geometry for CdTe at room temperature

B: Expression for " $f$ " in the High-field limit

Paget et. al. give the expressions for the hyperfine and quadrupolar relaxation rates as[39]:

$$\frac{1}{T_{1H}} = \Gamma(\gamma_N b_e(r))^2 \frac{2\tau_H}{1+\omega_H^2\tau_H^2} \tag{B1}$$

$$\frac{1}{T_{1Q}} = \Gamma(1-\Gamma)(\gamma_N b_q[E_{off}(r) - E_{on}(r)])^2[\frac{2K_1(\theta)\tau_Q}{1+\omega_1^2\tau_Q^2} + \frac{2K_2(\theta)\tau_Q}{1+\omega_2^2\tau_Q^2}] \tag{B2}$$

In the high magnetic field limit, where $\omega_H\tau_H$ , and $\omega_1\tau_Q$ and $\omega_2\tau_Q$ are much larger than one, these expressions become:

$$\frac{1}{T_{1H}} = \frac{2\Gamma(\gamma_N b_e(r))^2}{\omega_H^2\tau_H} \tag{B3}$$

$$\frac{1}{T_{1Q}} = \Gamma(1-\Gamma)(\gamma_N b_q[E_{off}(r) - E_{on}(r)])^2[\frac{2K_1(\theta)}{\omega_1^2\tau_Q} + \frac{2K_2(\theta)}{\omega_2^2\tau_Q}] . \tag{B4}$$

And

$$f = \frac{T_{1Q}}{T_{1H}} = \frac{1}{1-\Gamma}\frac{b_e^2(r)}{[b_Q(E_{off}(r) - E_{on}(r))]^2\omega_H^2}(\sum_i \frac{K_i}{\omega_i})^{-1}\frac{\tau_Q}{\tau_H} . \tag{B5}$$

Given,

$$\frac{1}{\tau_H} = \sigma_e v n \tag{B6}$$

$$\frac{1}{\tau_Q} = \frac{1}{\tau_r} + \sigma_e v n \tag{B7}$$

$$\Gamma = \frac{\sigma_c\tau_r v n}{1+\sigma_c\tau_r v n} . \tag{B8}$$

We get

$$f = \frac{1}{1-\Gamma}\frac{b_e^2(r)}{[b_Q(E_{off}(r) - E_{on}(r))]^2\omega_H^2}(\sum_i \frac{K_i}{\omega_i})^{-1}\frac{\sigma_e}{\sigma_c} . \tag{B9}$$

Rearrange, we get

$$f = f_0 \frac{\Gamma}{1-\Gamma} F(r,\theta), \tag{B10}$$

with

$$F(r,\theta) = \frac{e^{-4(r/a_0-1)}(r/a_0)^4}{[1-(1+2r/a_0+2r^2/a_0^2)e^{-2r/a_0}]^2(1-3\cos^2(\theta))}, \tag{B11}$$

and $f_0$ is a constant.

Bibliography


[1] Wolfgang Pauli, *Naturwiss*, **12,** 741 (1924).
[2] Walther Gerlach and Otto Stern, *Zeitschrift für Physik A Hadrons and Nuclei*, Volume **9**, Number 1, 353-355.
[3] G. E. Uhlenbeck and S. Goudsmit, *Naturwissenschaften* **47**, 953 (1925).
[4] I. Zutic, J. Fabian, and S. Das Sarma, *Rev. Mod. Phys.* Vol **76**, 323 (2004).
[5] I. I. Rabi, J. R. Zacharias, S. Millman, P. Kusch, *Phys. Rev.* **53** 318 (1938).
[6] A. Abragam, *The Principles of Nuclear Magnetism*, Oxford University Press, New York (1961).
[7] S. Sykora, Stan's Library, Vol I (2005) (http://www.ebyte.it/library/docs/nmr05b/NMR_SN_Perspectives.html).
[8] G. Lampel, *Phys. Rev. Lett.*, **20**, 491 (1968).
[9] S. E. Barrett, R. Tycko, L. N. Pfeiffer, and K. W. West, *Phys. Rev. Lett.* **72,** 1368 (1994).
[10] S. E. Barrett, G. Dabbagh, L. N. Pfeiffer, K. W. West, and R. Tycko, *Phys. Rev. Lett.* **74**, 5112 (1995).
[11] R. Tycko, S. E. Barrett, G. Dabbagh, L. N. Pfeiffer, and K. W. West, *Science* **268**, 1460 (1995).
[12] T. Pietrass, A. Bifone, T. Room, and E. L. Hahn, *Phys. Rev. B* **55**, 4050 (1997).
[13] P. L. Kuhns, A. Kleinhammes, T. Schmiedel, W. G. Moulton, P. Chabrier, S. Sloan, E. Hughes, and C. R. Bowers, *Phys. Rev. B* **55**, 7824 (1997).
[14] C. R. Bowers, *Solid State Nucl. Magn. Reson.* **11**, 11 (1998).
[15] A. K. Paravastu, S. E. Hayes, B. E. Schwickert, L. N. Dinh, M. B. Balooch, and J. A.Reimer, *Phys. Rev. B* **69**, 075203 (2004).
[16] A. K. Paravastu and J. A. Reimer, *Phys. Rev. B* **71**. 045215 (2005).
[17] S. E. Hayes, S. Mui, and K. Ramaswamy, *J. Chem. Phys* **128**, 052303 (2008).
[18] Y. Li, J. P. King, L. Peng, M. C. Tamargo, J. A. Reimer, and C. A. Meriles, *Appl. Phys. Lett.* **98**, 112101 (2011).
[19] C. A. Michal ad R. Tycho, *Phys. Rev. Lett.* **81**, 3988 (1998).
[20] C. A. Michal ad R. Tycho, *Phys. Rev. B.* **60**, 8672 (1999).
[21] A. Patel, O. Pasquet, J. Bharatam, E. Hughes, and C. R. Bowers, *Phys. Rev. B.* **60**, R5105 (1999).
[22] T. Pietrass and M. Tomaselli, *Phys. Rev. B* **59**, 1986 (1999).
[23] I. J. H. Leung and C. A. Michal, *Phys. Rev. B* **70**, 035213 (2004).
[24] W. Dong, B. Li, Q. Zhang, M. C. Tamargo, and C. A. Meriles, *Phys. Rev. B* **80**, 045211 (2009).
[25] P. Khandelwal, N. N. Kuzma, S. E. Barrett, L. N. Pfeiffer, and K. W. West, *Phys. Rev. Lett.* **81**, 673 (1998).
[26] R. Tycko, *Mol. Phys.* **95**, 1169 (1998).
[27] Meier and Zakharchenya, 1984.
[28] W. Happer, *Rev. Mod. Phys.* **44**, 169 (1972).
[29] D. A Van Baak, *Am. J. Phys*. **64**, 6 (1996).
[30] T. Pietrass, A. Bifone, T. Room, and E. L. Hann, *Phys. Rev. B* **53**, 4428 (1996).
[31] P. L. Kuhns, A. Kleinhammes, T. Schmiedel, W. G. Moulton, P. Chabrier, S. Sloan, E. Hughes and C. R. Bowers, *Phys. Rev. B* **55**, 7825 (1997).
[32] http://www.ioffe.rssi.ru/SVA/NSM/Semicond/GaAs/bandstr.html#Temperature
[33] J. M. Kikkawa and D. D. Awschalom, Science **287,** 473 (2000).
[34] G. Salis, D. T. Fuchs, J. M. Kikkawa, D. D. Awschalom, Y. Ohno, and H. Ohno, *Phys.*

*Rev. letts.* **86**, 2766 (2001).
[35] H. Sanada, Y. Kondo, S. Matsuzaka, K. Morita, C. Y. Hu, Y. Ohno, and H. Ohno, *Phys. Rev. Letts.* **96**, 067602 (2006).
[36] Y. Kondo, M. Ono, S. Matsuzaka, K. Morita, H. Sanada, Y. Ohno, and H. Ohno, *Phys. Rev. Letts* **101**, 207601 (2008).
[37] S. Mui, K. Ramaswamy, C. J. Stanton, S. A. Crooker, and S. E. Hayes, *Phys. Chem. Chem. Phys.* **11**, 7031 (2009).
[38] P. Coles and J. A. Reimer, *Phys. Rev. B* **76**, 174440 (2007).
[39] D. Paget, T. Amand, and J.-P. Korb, *Phys. Rev. B* **77**, 245201 (2008).
[40] D. Paget, *Phys. Rev. B* **25**, 4444 (1982).
[41] W. E. Blumberg, *Phys. Rev*. **119**, 79 (1960).
[42] P. G. De Gennes, *J. Phys. Chem. Solids* **7**, 345 (1958).
[43] G. R. Khutsishvili, *Usp. Fiz. Nauk* **87**, 211 (1965) [*Sov. Phys. Usp*. **8**, 743 (1966)].
[44] M. E. Nowakowski, G. D. Fuchs, S. Mark, N. Samarth, and D. D. Awschalom, *Phys. Rev. Lett.* **105**, 137206 (2010).
[45] R. K. Kawakami, Y. Kato, M. Hanson, I. Malajovich, J. M. Stephens, E. Johnston-Halperin, G. Salis, A. C.Gossard, and D. D. Awschalom, *Science* **294**, 131 (2001).
[46] J. Reimer, *Solid State Nucl. Magn. Reson.* **37**, 3 (2010).
[47] M. R. Fitzsimmons, B. J. Kirby, N. W. Hengartner, F. Trouw, M. J. Erickson, S. D. Flexner, T. Kondo, C. Adelmann, C. J. Palmstrom, P. A. Crowell, W. C. Chen, T. R. Gentile, J. A. Borchers, C. F. Majkrzak, and R. Pynn, *Phys. Rev. B* **76**, 245301 (2007).
[48] P. Y. Yu and M. Cardona, 2001.
[49] A. Goto, S. Ohki, K. Hashi, and T. Shimizu, *Nature Comm.* **2**, 378 (2011).